LINEAR LONGITUDINAL OSCILLATIONS IN COLLISIONLESS PLASMA DIODES WITH THIN SHEATHS. PART II. APPLICATION TO AN EXTENDED PIERCE-TYPE PROBLEM

by

S. Kuhn

Memorandum No. UCB/ERL M83/61

3 October 1983

ELECTRONICS RESEARCH LABORATORY

College of Engineering
University of California, Berkeley
94720

LINEAR LONGITUDINAL OSCILLATIONS IN COLLISIONLESS PLASMA DIODES WITH THIN SHEATHS. PART II. APPLICATION TO AN EXTENDED PIERCE-TYPE PROBLEM

S. Kuhn[a)]

Plasma Theory and Simulation Group, Electronics Research Laboratory, University of California, Berkeley, CA 94720

The integral-equation method developped in Part I is applied to a Pierce-type diode (Pierce 1944) whose external circuit involves a resistor, an inductor, and a signal generator. The general linear perturbational problem is solved analytically for the small-amplitude quantities $\tilde{j}_e(t)$ (external-circuit current density) and $\tilde{E}(x,t)$ (electrostatic field). Each of these quantities can be constructed from a "spatial" Green's function (describing initial perturbations of the plasma), a "temporal" Green's function (describing external-generator signals), and two functions associated with the initial state of the external circuit. The solutions generally exhibit an initial transient and an asymptotic part, the latter being a superposition of eigenmodes only. Systematic numerical results for eigenfrequencies and eigenmode profiles in some typical parameter regions demonstrate that the linear response and stability behavior of the diode system may substantially depend on the properties of the external circuit.

[a)] Permanent address: Institute for Theoretical Physics, University of Innsbruck, A-6020 Innsbruck, Austria

I. INTRODUCTION AND SUMMARY

This paper constitutes Part II of a study proposing an integral-equation approach to linear longitudinal oscillations in collisionless plasma diodes with thin sheaths. The method was formally developed in Part I[1] and is comprehensive in that it (i) handles the combined initial-value and external-perturbation problem, thus including the eigenmode problem as a special case, and (ii) allows for explicit and simultaneous inclusion of three basic constituents of bounded plasma systems, namely the plasma itself, the boundaries, and the external circuit. As discussed in Subsec. III.A/I,[2] the present restriction to one-dimensional diode geometry is not inherent to the integral-equation approach as such and is likely to become dispensable at a later stage of development of the theory.

In the present paper, the method developed in Part I is employed to solve an extended Pierce-type problem involving a non-trivial external circuit. Our goal is (i) to demonstrate the applicability and handling of the method, and (ii) to show in numerical detail that the external circuit, an essential part of any bounded plasma system, may crucially influence the overall dynamic and stability behavior. The paper proceeds as follows.

Section II gives a description of the Pierce problem[3–39] and some of its implications. From the discussion and literature survey in Subsec. II.A it is concluded that Pierce-type instabilities are of great practical importance, e.g., in various laboratory plasma devices, and have recently attracted considerable interest in the context of such modern concepts and applications as double layers or inertial confinement fusion. Areas are pointed out in which more work is needed, among them the complexes of external-circuit effects and plasma-wall interaction. In Subsec. II.B we present an argument according to which

the Pierce diode represents, under certain circumstances, a rough but still useful first approximation to the one-emitter plasma diode or single-ended Q machine.

In Sec. III, the method developed in Part I is formally applied to derive the integral equations governing the extended Pierce-type problem considered, which differs from the "classical" (i.e., short-circuited) one[3] in that it includes an external circuit involving a signal generator, a resistor, and an inductor as shown in Fig. 1. Subsection III.A gives the formal specifications of this perturbational problem, i.e., the level-one quantities defined in Table I/I. In Subsec. III.B we try to foresee the structure of the result and conclude that the general solution can be obtained by linear superposition of four different types of "basic modes", two of which are identical with the "spatial" and the "temporal" Green's functions, respectively. The level-two through level-four quantities of Table I/I are calculated in Subsec. III.C and used in Subsec. III.D to explicitly construct the integral equations (37)/I–(40)/I as well as the equivalent matrix equation (48)/I. For the particular case under consideration, this system turns out to reduce to just two integral equations, the unknowns being the Laplace-transformed perturbations $\tilde{j}_e(\omega)$ (external-circuit current density) and $\tilde{E}(x,\omega)$ (electrostatic field).

In Subsec. IV.A, these integral equations are solved for the Laplace- transformed basic modes, which are Laplace inverted in Subsec. IV.B into the time-dependent basic modes. This completes the general solution of the combined external-perturbation and initial-value problem. Each of the basic modes exhibits an initial transient as well as an asymptotic part and can be represented as a linear superposition of eigenmodes. The related eigenfrequencies are the

zeros of the characteristic equation (or "dispersion relation"), whose unnormalized form is given by Eq. (45).

The nondimensional eigenmode problem is dealt with analytically in Sec. V, and numerically in Sec. VI. In Subsec. V.A, the characteristic equation is re-written in nondimensional form and found to depend on the three dimensionless parameters α ("Pierce parameter"), ρ (external-circuit resistance), and λ (external-circuit inductance). In Subsecs. V.B and V.C we discuss some analytic properties of the eigenfrequencies and eigenmode profiles, respectively.

Throughout Sec. VI, the classical, short-circuited Pierce diode[3] ($\alpha > 0, \rho = 0, \lambda = 0$) is used as a standard reference to which all other cases are conveniently compared. It is reviewed in Subsec. VI.A, where numerical data describing its eigenfrequencies and eigenmode structures in three typical α-intervals are presented, and a classification scheme for the eigenfrequencies is introduced. Subsection VI.B deals with the "purely resistive" case ($\alpha > 0, \rho > 0, \lambda = 0$) and demonstrates that finite external-circuit resistance can, among other things, stabilise a classically unstable mode and change the character of the dominant mode from oscillatory to non-oscillatory. In the "purely inductive" case ($\alpha > 0, \rho = 0, \lambda > 0$), which is considered in Subsec. VI.C, we find a new oscillatory mode which may completely change the linear dynamic behavior and even become unstable for α-values at which the classical Pierce diode is stable. Some general aspects and implications are discussed in Subsec. VI.D.

Finally, our main conclusions are summarized in Sec. VII.

II. THE PIERCE PROBLEM

A. Pierce diode and Pierce instability

The plasma diode model given by Pierce about fourty years ago,[3] which has ever since been reconsidered in various modifications,[4–39] is a particularly simple special case of the collisionless one-dimensional configurations described in Subsec. II.A. The ions, which are assumed to be immobile, provide a uniform neutralizing background of density $\bar{n}_p$, immersed between the left-hand ($x = 0$) and right-hand ($x = L$) electrodes. The electrons are constantly injected at the left-hand electrode as a cold beam with density $\bar{n}_p$ and velocity $\bar{v}$, and are absorbed when hitting either electrode. Both electrodes are invariably kept at the same potential, which corresponds to assuming an external short-circuit.

In what follows, the system just described will be called the "classical" Pierce diode. Out of the various equilibrium states the classical Pierce diode can exhibit, the original Pierce paper[3] was only concerned with the one in which the electrons are uniform as well. This special case will be referred to as the "uniform classical" one.

Nondimensional analysis shows that the equilibrium ($\partial/\partial t = 0$) and dynamic states of the classical Pierce diode can be conveniently classified in terms of the single parameter

$$\alpha \equiv \frac{\omega_p L}{\bar{v}} \tag{1}$$

where $\omega_p = (4\pi\bar{n}_p e^2/m)^{\frac{1}{2}}$ is the electron plasma frequency, e is the positive elementary charge, and m is the electron mass. The parameter α, henceforth referred to as "Pierce parameter", is proportional to the ratio of electron transit

time to electron plasma period and thus provides a rough measure of the relative importance of plasma versus boundedness effects.

In contrast to the classical Pierce diode, any similar plasma configuration characterized by a strong electron current between two electrodes will be referred to as "Pierce-type" or "modified Pierce" diode. Pierce-type configurations, although not always recognized as such, are widely encountered in practice, cf. below.

Despite its simplicity and degeneracy, the uniform classical Pierce diode is of fundamental importance because it qualitatively retrieves some typical bounded-system behavior yet is still tractable—to some extent, at least—with reasonable mathematical effort. Most importantly, it exhibits the "Pierce instability", which destroys the electron equilibrium more or less violently, depending on the value of α. Numerical data for the classical Pierce instability may be found, e.g., in Ref. 33, Ref. 34, and Subsec. VI.A below.

Since the classical Pierce instability disappears in the infinite-plasma limit (i.e., for $L \to \infty$, and hence $\alpha \to \infty$), it is inherently due to the finite, bounded character of the system. One reason for this striking difference between finite/bounded and infinite/unbounded systems can be spotted in the different energetics: For a shorter diode, the energy exchanged with the electrodes via particle injection and absorption is of greater relative importance, so that the system may rapidly evolve to a final state whose time-averaged energy is significantly different as compared to the initial one; if the diode becomes sufficiently long, this energy exchange is relatively unimportant and so the initial energy is practically conserved. A second important difference comes about through the external circuit, whose main effect is to control the surface charges sitting on

the electrodes. These surface charges give rise to a vacuum field that is superimposed on the space-charge field of the plasma and is inversely proportional to the diode length L, thus becoming less effective for a longer diode.

The Pierce instability may, generally speaking, occur in any Pierce-type system but will usually not be as violent as in the idealized classical case. Whenever it appears it is likely to play a non-negligible or even dominant role in the linear and/or nonlinear dynamics of the system. It may, e.g., cause a rapid overall transition of the electron and potential distributions to a new, "temporary" equilibrium state, which, after reaction of the ions on their much longer time scale, can result in double layers,[22,24,27,35,38,42] phase-space holes,[30,35] or relaxation oscillations.[7–9,11,15,17,18,25,29,41,42] The Pierce instability may alternatively give rise to electron turbulence[30,34,43] which, in turn, can influence the ion dynamics via the ponderomotive force. In all cases, the Pierce instability sets an upper limit to the time-averaged electric current that can be passed through the system.

In short, the Pierce instability is not just of academic interest but rather requires serious consideration whenever one is dealing with bounded, current-carrying, weakly collisional plasma systems. It has, accordingly, been invoked in the context of various practical applications and devices such as electron-beam generation,[19,20] microwave generation[19,33,34] and amplification,[19] thermionic converters,[7–9,11,15,18,25,29] drift tubes,[13] triode lasers,[10] or ion-beam neutralization for inertial-confinement fusion.[31,32,37,39] Its relevance to low-density single-ended Q machines[41,42] is discussed in Subsec. II.B below. Experimental evidence of the Pierce instability can be found, e.g., in Refs. 5, 11, 22, 27, and 40–42.

Since the appearance of the classical Pierce paper,[3] numerous extensions and modifications of the Pierce instability have been studied analytically[3–6,8,10,12–14,16–23,26,27,29–37,39] and numerically.[7,9,11,15,24,25,28,30–32,38] These studies were based on fluid,[3–5,10,12–14,16–20,22,23,27,30–35,37,39] kinetic,[6,8,21,25,26,28,29,36,38] or particle[7,9,11,15,24,30–32] models. Beams of finite thermal spread were considered in Refs. 6–9, 11, 15, 21, 23–26, 28–30, 32, 36, 38, and 39, and effects of finite ion mass were dealt with in Refs. 4, 7–13, 15, 17, 22–24, 27, 28, 31, 36, and 38. Apart from a few remarks on collisional effects in Ref. 10, all papers mentioned considered the collisionless case only. Most studies were concerned with one-dimensional geometry; two-dimensional effects were considered in Refs. 3, 5, 13, 20, 31, and 32, but no three-dimensional treatment is known to us. Non-uniform equilibria were admitted in Refs. 6–9, 11, 12, 15, 18, 19, 21, 24–26, 28–31, 34, and 38. Both linear[3–6,8,10,12,13,17–23,26,27,29–33,36,37,39] and nonlinear[7,9,11,14–16,24,25,28,30–32,34,38] properties of the Pierce instability have been studied. Except for some considerations on electromagnetic effects in Ref. 13, all references cited employ the electrostatic approximation.

Given the fair amount of literature that already exists on the Pierce instability, the question arises as to what remains to be done. In our opinion, there are two basic lines along which progress can—and should—be made. (i) Several areas can be located in which, to our knowledge, very little detailed work has been done. E.g., the role of non-trivial external-circuit elements, though pointed out to be potentially important,[12] has been given consideration by only very few authors.[8,12,19,37,38] Another example is the fact that there does not seem to exist any treatment including realistic plasma-wall interaction

processes such as inelastic reflection or secondary-particle emission. As a third example we wish to mention that only little analytic work has been devoted to the nonlinear properties of the Pierce instability,[14,16,34,35] which, however, indicates that this is a promising area where much more progress could be made. (ii) In view of the complexity of realistic systems, it seems desirable to proceed towards treatments including more of the relevant physics simultaneously. E.g., all linear analyses available are concerned with the eigenmode problem—i.e., with a time dependence $\exp(\alpha t)$—rather than with the full initial-value and external-excitation problem.

Generally speaking, we believe that the fundamental importance of the Pierce problem requires and justifies further theoretical efforts towards a more complete understanding. Thus, the present paper contributes to two aspects which, according to the above literature survey, have not yet been treated to a significant extent: (i) The complete initial-value and external-perturbation problem is solved in Secs. IV and V, and (ii) a fair amount of systematic numerical data describing the influence of external-circuit resistance and external-circuit inductance on the linear eigenfrequencies and eigenmode profiles is presented in Sec. VI. The results of particle simulations extending into the nonlinear regimes of the Pierce instability will be presented elsewhere.[43]

B. Cold-beam, thin-sheath approximation of the positively biased one-emitter plasma diode or single-ended Q machine

In this subsection we are concerned with the well-known one-dimensional model of the collisionless one-emitter plasma diode considered, e.g., in the context of thermionic converters[44,45] or low-density single-ended Q machines.[46–48]

Our goal here is to demonstrate that the positive-bias equilibrium states of this model can, to a certain extent, be approximated by the uniform classical Pierce configuration.[3] This argument is of practical importance because it allows one to obtain, with relative ease, quantitative estimates of stability domains and linear growth rates. Moreover, the numerical results following from this model seem to indicate that, under normal operation conditions, single-ended Q machines should always be Pierce unstable, a fact which apparently has not been pointed out previously but could possibly be of relevance in explaining the various dynamic phenomena observed experimentally.[41-42] For details of the model, the reader is referred to Refs. 44–48 and many others cited there.[49]

The equilibrium states in question are characterised by the potential distribution types 1 (monotonically increasing) and 2 (one-minimum) as defined in Fig. 3 of Ref. 46 and Fig. 1a of Ref. 48.[49] For both of these distribution types, the plasma potential $\bar{V}_p$ is positive with respect to that of the emitter surface, $\bar{V}(x = 0) = 0$. Hence, the electrons—which are assumed to leave the emitter surface with a half Maxwellian velocity distribution—always enter the plasma region as a distinct beam with a truncated Maxwellian distribution. The cut-off velocity, average velocity, and effective temperature of this distribution are respectively given by[48]

$$\bar{v}_c = \left[2e(\bar{V}_p - \bar{V}_m)/m\right]^{\frac{1}{2}} \tag{2a}$$

$$\bar{v}_{av} = \left(\frac{2\kappa T}{\pi m}\right)^{\frac{1}{2}} \frac{\exp\left(-m\bar{v}_c^2/2\kappa T\right)}{\operatorname{erfc}\left[\bar{v}_c(m/2\kappa T)^{\frac{1}{2}}\right]} \tag{2b}$$

$$\bar{T}_{eff} = T\left[1 - \frac{m}{\kappa T}\bar{v}_{av}(\bar{v}_{av} - \bar{v}_c)\right] \tag{2c}$$

where $\bar{V}_m$ is the minimum potential (cf. Fig. 1/I; for a monotonically increasing potential distribution as shown in Fig. 1 we have $\bar{V}_m = 0$), κ is Boltzmann's constant, T is the emitter temperature, and erfc is the complementary error function. For a "long" system such as the Q machine, the nondimensional quantities $\bar{T}_{eff} = T_{eff}/T$, $\bar{\varphi}_c = \bar{v}_c/v_s$ (where $v_s = (2\kappa T/m)^{\frac{1}{2}}$), and $\bar{\varphi}_{av} = \bar{v}_{av}/v_s$, as well as several others, depend only on the "neutralization parameter" $\bar{\alpha}$, which is defined as the ratio of desorbing-ion over emitted-electron density at the emitter surface.[46-49] Figure 2b of Ref. 48 shows that at $\bar{\alpha} = 0.405$—i.e., at the transition between one-minimum and monotonically increasing potentials—$\bar{T}_{eff}$ assumes its maximum ($\simeq 0.22$), whereas $\bar{\varphi}_c$ and $\bar{\varphi}_{av}$ assume their respective minima ($\simeq 0.59$ and $\simeq 0.98$, respectively). Hence, the cold-electron-beam approximation is least accurate, though still acceptable for a first estimate, for $\bar{\alpha} = 0.405$; it becomes better with decreasing or increasing $\bar{\alpha}$ because in both cases the velocity spread decreases while the beam velocity increases.

The thin-sheath approximation made throughout this work requires that the axial extensions of both the emitter and the collector sheaths be much smaller than that of the plasma region. In a Q machine, this condition is usually satisfied, except when the collector bias is raised to excessively high values.[50,51] Quantitative estimates of collector sheath widths can be obtained, e.g., from Fig. 3 of Ref. 48.

In accordance with the foregoing considerations, we now replace a long one-emitter diode of the above kind with an "approximate" diode having infinitely thin sheaths and a uniform plasma region of length L. The electrons of the approximate diode form a cold beam whose plasma density and velocity

are respectively equal to the plasma density and average velocity of the original diode. Apart from the non-trivial external circuits we have in mind, this approximate diode is formally identical with the uniform classical Pierce diode described in Subsec. II.A. One can thus associate with it a Pierce parameter α as defined by Eq. (1). In an extension of the concepts introduced in Ref. 48, we now propose a method yielding quantitative estimates of α. This establishes a link between experimental operating conditions and theoretical results such as given in Sec. VI and elsewhere.[33,34]

In terms of standard nondimensional quantities,[48,49] Eq. (1) can be rewritten in the form

$$\frac{\alpha}{\Lambda} = \left(\frac{\mathcal{D}_p}{2\bar{\varphi}_{av}^2}\right)^{\frac{1}{2}} \tag{3}$$

where $\mathcal{D}_p = \bar{n}_p/n_s$ is the normalized plasma density,

$$n_s = \frac{A_c^*}{e}\left(\frac{\pi m}{2\kappa}\right)^{1/2} T^{3/2} \exp\left(\frac{eW_c^*}{\kappa T}\right)$$

is the Richardson emission density, A_c^* and W_c^* are the effective Richardson constant and work function for thermal electron emission from the emitter, $\Lambda = L/l_s$ is the normalized system length, and $l_s = (\kappa T/4\pi n_s e^2)^{1/2}$ is the scaling length. With the numerical results displayed in Fig. 2b of Ref. 48 we have calculated (α/Λ) as a function of the neutralization parameter, the result being shown in Fig. 2.

For a given experimental situation, the Pierce parameter α can now be obtained as follows. With the method proposed in Sec. 3 of Ref. 48, one first determines $\bar{\alpha}$ and Λ. One then finds, by inspection of Fig. 2, the appropriate value of $(\bar{\alpha}/\Lambda)$, which, upon multiplication by Λ, yields the desired result.

In order to get a feeling for the numbers that may occur in practice, we find it useful to consider yet another representation. Multiplying both sides of Eq. (3) by l_s, we obtain

$$\frac{\alpha}{L} = \frac{1}{l_s}\left(\frac{\alpha_p}{\Lambda}\right), \tag{4}$$

which quantity is to be plotted against the equilibrium plasma density. Figure 3 shows several curves (α/L) versus $\bar{n}_p$, each curve corresponding to a specific emitter temperature. The emitter material assumed is tungsten with a Richardson constant $A_e^* = 120\,\mathrm{A\,cm^{-2}\,K^{-2}}$ and effective work functions for electron emission and surface ionization $W_e^* = W_i^* = 4.52\,\mathrm{V}$, cf. Fig. 3a of Ref. 47. Each curve has an upper and a lower branch, corresponding to one-minimum and monotonically increasing potentials, respectively. The arrows indicate the direction of increasing $\bar{\alpha}$. These curves can be interpreted as follows. Consider a diode with $L = 20\,\mathrm{cm}$ and $T = 2200\,\mathrm{K}$, and assume that the method of Ref. 48 has predicted a one-minimum equilibrium distribution with $\bar{n}_p = 1.1\times10^7\,\mathrm{cm^{-3}}$. From Fig. 3 we find $(\alpha/L = 2.6\,\mathrm{cm^{-1}}$, and hence $\alpha = 52 = 16.6\pi$. Upon solving the characteristic equation (Subsec. V.A) we would find that there are, in the short-circuit case, two unstable eigenmodes with frequencies $\omega_1 = (0.035+0.032i)\omega_p$ and $\omega_2 = (0.13+0.0025i)\omega_p$. However, anticipating the results of Subsec. VI.B we expect that both of these modes can be stabilized by, e.g., inserting a sufficiently large resistance into the external circuit.

Generally speaking, the curves plotted in Fig. 3 suggest that, for typical operation conditions, the Pierce parameter α will usually lie well above π, so that, in the short-circuit case, the positively biased single-ended Q machine should always be Pierce unstable. In fact, the experimental evidence is that

it is always unstable[41,42] except for very high collector biases,[50,51] but at the present stage of understanding it does not seem possible to clearly indicate the dominant instability mechanism. E.g., it has been pointed out[48,52] that the positively biased single-ended Q machine may be Buneman unstable as well, but the results there were obtained in the infinite-plasma approximation and therefore have only preliminary character. For large values of α, the growth rates of the classical Pierce instability become much smaller than the plasma frequency, cf. Subsec. VI.A. They can, moreover, be modified by a number of components such as external-circuit elements, plasma-wall interaction processes, finite sheath widths, collisions, finite velocity spreads, or two-dimensional geometry. If, however, α is not too far above π, the Pierce instability is likely to manifest itself more clearly, and the theoretical results given in Subsec. VI. may not be all too unrealistic.

In any case, we believe that the present understanding of bounded plasma systems—even of relatively simple ones—is far from complete, and that much more theoretical and experimental work will be needed to improve this situation to a significant extent.

III. DERIVING THE INTEGRAL EQUATIONS

A. Specifications (level-one quantities)

In this subsection we formally define the perturbational problem to be solved. The level-one quantities as listed in Table I/I are specified in accordance with the general description of the problem given in Secs. I and II.

We restrict ourselves to considering "electron" phenomena, i.e., phenomena sufficiently fast that the ions are practically unable to react and hence can be considered to be immobile. Thus, the electrons are the only species we have to deal with ($n_\sigma = 1$), and the species superscript σ can be dropped.

In the plasma region, the equilibrium velocity distribution function of the electrons is assumed to be

$$\bar{f}(v) = \bar{n}_p\, \delta(v - \bar{v})\,, \tag{5}$$

which corresponds to a cold electron beam of density $\bar{n}_p$, travelling to the right with velocity $\bar{v}$.

Let the initial perturbation of the electron distribution function be of the form

$$\tilde{f}_i(x, v) = \tilde{f}_{\xi i}\, \delta(x - \xi)\, \delta(v - \bar{v})\,. \tag{6}$$

This means that the final solution will, among other things, contain the "spatial" Green's function of the problem, from which the solution for any arbitrary initial perturbation profile can be easily constructed by suitable integration over ξ, cf. Subsec. III.B.

The boundary conditions for the particles are specified by requiring constant (non-zero) emission at the left-hand electrode ($\tilde{f}_l(v > 0, t) = 0$), and con-

stant (zero) emission at the right-hand electrode ($\tilde{f}_r(v<0,t)=0$). In terms of the functions introduced in Eq. (26)/I, these conditions can be expressed as

$$\tilde{f}_{lg}(v>0,t)=0 \tag{7a}$$

$$b_l^{\sigma\sigma'}(v>0,v'<0)=0 \tag{7b}$$

$$\tilde{f}_{rg}^{\sigma}(v<0,t)=0 \tag{7c}$$

$$b_r^{\sigma\sigma'}(v<0,v'>0)=0\,. \tag{7d}$$

The exemplary external circuit we consider consists of a d.c. voltage source shaping the equilibrium, a small-signal generator SG, a resistance $\hat{R}$, and an inductance $\hat{L}$, all connected in series as shown in Fig. 1. (Clearly, $\hat{R}$ and $\hat{L}$ are defined per unit cross-section area.) For this system, the external-circuit condition (33)/I combined with the potential-balance equation (35)/I reads

$$\begin{aligned}\Delta\tilde{V}_e(t) &= \Delta\tilde{V}_p(t)\\ &= \tilde{V}_{e\tau}\delta(t-\tau)+\hat{R}\tilde{j}_e(t)+\hat{L}\frac{d}{dt}\tilde{j}_e(t)\,,\end{aligned} \tag{8}$$

where SG has been assumed such as to produce a delta-function signal at time τ, with $\tau>0$. Thus, the solution will also contain the "temporal" Green's function, from which one may ultimately obtain the solution for any arbitrary external signal $\tilde{V}_e(\tau)$, cf. Subsec. III.B.

In order to completely specify the initial state of the external circuit (and, hence, of the whole diode system), one has to prescribe either two of the three initial values $\tilde{j}_{ei}$, $(d\tilde{j}_e/dt)_i$, and $\Delta\tilde{V}_{pi}$, whence the third one is readily obtained via (8). In what follows, $\tilde{j}_{ei}$ and $(d\tilde{j}_e/dt)_i$ will be assumed to be given.

Following the method developped in Part I, the initial-value and external-perturbation problem just defined must be solved simultaneously for the functions $\tilde{j}_e(t)$, $\tilde{E}(x,t)$, $\tilde{f}_l(v>0,t)$, and $\tilde{f}_r(v<0,t)$. However, since we have

prescribed the two latter functions to vanish identically, the problem actually reduces to finding $\tilde{j}_e$ and $\tilde{E}$.

B. Basic modes and general solution

The linear perturbational problem specified in Subsec. III.A involves the four amplitude factors $\tilde{f}_{\xi i}$, $\tilde{V}_{er}$, $\tilde{j}_{ei}$, and $(d\tilde{j}_e/dt)_i$, which can be prescribed independently of each other. Hence we conclude that the solution will be a linear superposition of four independent "basic" modes, which we choose to define as shown in Table I. These basic modes must not be confused with the eigenmodes discussed in Sec. V; they rather involve sperpositions of eigenmodes, cf. Sec. IV. Basic modes 1 and 2 are the spatial and temporal Green's functions, respectively, whereas basic modes 3 and 4 are connected with the initial state of the external circuit.

As opposed to the basic-mode problem specified in Subsec. III.A and solved in Sec. IV, the general perturbational problem for the Pierce-type configuration considered is obtained by replacing (6) with

$$\tilde{f}_i(x,v) = \tilde{f}_i(x)\,\delta(v-\bar{v}) \tag{9}$$

and (8) with

$$\begin{aligned}\Delta\tilde{V}_e(t) &= \Delta\tilde{V}_p(t) \\ &= \tilde{V}_e(t) + \hat{R}\tilde{j}_e(t) + \hat{L}\frac{d\tilde{j}_e(t)}{dt}\end{aligned} \tag{10}$$

where the initial perturbation profile $\tilde{f}_i(x)$ and the external-generator signal $\tilde{V}_e(t)$ are now arbitrary. The solution to this problem can be constructed by linear superposition of basic modes in the form

$$\begin{pmatrix} \tilde{j}_e(t) \\ \tilde{E}(x,t) \end{pmatrix} = \int_0^L d\xi\, \tilde{f}_i(\xi) \begin{pmatrix} \hat{j}_e^{(1)}(t|\xi) \\ \hat{E}^{(1)}(x,t|\xi) \end{pmatrix} + \int_0^t d\tau\, \tilde{V}_e(\tau) \begin{pmatrix} \hat{j}_e^{(2)}(t|\tau) \\ \hat{E}^{(2)}(x,t|\tau) \end{pmatrix} + \tilde{j}_{ei} \begin{pmatrix} \hat{j}_e^{(3)}(t) \\ \hat{E}^{(3)}(x,t) \end{pmatrix} + \left(\frac{d\tilde{j}_e}{dt}\right)_i \begin{pmatrix} \hat{j}_e^{(4)}(t) \\ \hat{E}^{(4)}(x,t) \end{pmatrix} \tag{11}$$

Thus, solving the full problem is practically equivalent to finding the basic modes; only these will be dealt with in the rest of the present section and in Sec. IV.

C. Higher-level quantities

Starting from the level-one quantities specified in Subsec. III.A, we now construct the level-two through level-four quantities according to Table I/I. To this end it proves convenient to first introduce the auxiliary functions

$$R_1(x,\omega) = 1 + \frac{\omega_p}{2} \sum_{\beta=\pm} \frac{\beta}{\omega + \beta\omega_p} \left(\exp \frac{i(\omega + \beta\omega_p)x}{\bar{v}} - 1 \right) \tag{12a}$$

$$R_2(x,\omega|\xi) = \frac{\omega_p}{2} \sum_{\beta=\pm} \frac{1}{\omega + \beta\omega_p} \left(\exp \frac{i(\omega + \beta\omega_p)(x-\xi)}{\bar{v}} - 1 \right) \tag{12b}$$

$$R_3(\omega) = 1 + \frac{\bar{v}\omega_p}{2iL} \sum_{\beta=\pm} \frac{\beta}{(\omega + \beta\omega_p)^2} \left(\exp \frac{i(\omega + \beta\omega_p)L}{\bar{v}} - 1 - i\frac{\omega + \beta\omega_p}{\bar{v}} L \right) \tag{12c}$$

$$R_4(\omega|\xi) = \frac{\omega_p \bar{v}}{2iL} \sum_{\beta=\pm} \frac{1}{(\omega + \beta\omega_p)^2} \left(\exp \frac{i(\omega + \beta\omega_p)(L-\xi)}{\bar{v}} - 1 - i\frac{\omega + \beta\omega_p}{\bar{v}}(L-\xi) \right) \tag{12d}$$

$$R_5(x,\omega) = -\frac{x}{L} + i\frac{\omega_p \bar{v}}{2L} \sum_{\beta=\pm} \frac{\beta}{(\omega + \beta\omega_p)^2} \left(\exp \frac{i(\omega + \beta\omega_p)x}{\bar{v}} - 1 - i\frac{\omega + \beta\omega_p}{\bar{v}} x \right) \tag{12e}$$

which are non-singular for all values of ω.

Level two:

$$D(q,\omega) = 1 - \left(\frac{\omega_p}{q\bar{v}+\omega}\right)^2 = \frac{(q-q_-)(q-q_+)}{(q+\frac{\omega}{\bar{v}})^2} \tag{13}$$

with $q_\pm = -(\omega \pm \omega_p)/\bar{v}$,

$$\tilde{f}_i(q,v) = \tilde{f}_{\xi i}\, e^{iq\xi}\, \delta(v-\bar{v}) \tag{14}$$

$$\tilde{f}^{\sigma}_{lg}(v>0,\omega) = 0\,, \qquad \tilde{f}^{\sigma}_{rg}(v<0,\omega) = 0 \tag{15a,b}$$

$$\begin{aligned}\Delta\tilde{V}_e(\omega) &= \Delta\tilde{V}_p(\omega) \\ &= \left(\tilde{V}_{er}e^{i\omega\tau} - \hat{L}\tilde{j}_{ei}\right) + \left(\hat{R} - i\omega\hat{L}\right)\tilde{j}_e(\omega)\end{aligned} \tag{16}$$

$$\Delta\tilde{V}_{pi} = \hat{R}\tilde{j}_{ei} + \hat{L}\left(\frac{d\tilde{j}_e}{dt}\right)_i \tag{17}$$

Level three:

$$\tilde{E}_{li} = 4\pi e\tilde{f}_{\xi i}\left(1 - \frac{\xi}{L}\right) - \frac{\Delta\tilde{V}_{pi}}{L} \tag{18}$$

$$\tilde{k}_1(x,v,\omega) = i\frac{\bar{v}}{\omega_p}\tilde{f}_{\xi i}\, U(x-\xi)\,\delta(v-\bar{v})\, R_2(x,\omega|\xi) \tag{19}$$

$$k_2(x,\omega) = -iR_1(x,\omega) \tag{20}$$

$$k_6(x, v=\bar{v}, \omega) = \frac{\bar{v}}{2i\omega}\sum_{\beta=\pm}\exp\frac{i(\omega+\beta\omega_p)x}{\bar{v}} \tag{21}$$

(Remark: k_6 is only required for $v = \bar{v}$.)

$$\tilde{k}_7(v,\omega) = \tilde{f}_{\xi i}\exp\left(-i\frac{\omega}{\bar{v}}\xi\right)\delta(v-\bar{v}) \tag{22}$$

Level four:

$$\tilde{V}_{e0}(\omega) = \tilde{V}_{er}e^{i\omega\tau} - \hat{L}\tilde{j}_{ei} \tag{23a}$$

$$Z_e(\omega) = \hat{R} - i\omega\hat{L} \tag{23b}$$

$$k_5(x,\omega) = \frac{4\pi i}{\omega}R_1(x,\omega) \tag{24}$$

$$S_0(x,[x'],\omega) = 0 \tag{25}$$

$$\begin{aligned}\tilde{k}_8(x,\omega) = \tilde{f}_{\xi i}\left\{4\pi i e\left[\left(1-\frac{\xi}{L}\right)\frac{R_1(x,\omega)}{\omega} + U(x-\xi)\frac{R_2(x,\omega|\xi)}{\omega_p}\right]\right\} \\ + \tilde{V}_{er}\{0\} + \tilde{j}_{ei}\left\{\frac{\hat{R}}{i\hat{L}}\frac{R_1(x,\omega)}{\omega}\right\} + \left(\frac{d\tilde{j}_e}{dt}\right)_i\left\{\frac{\hat{L}}{i\hat{L}}\frac{R_1(x,\omega)}{\omega}\right\}\end{aligned} \tag{26}$$

$$S_l(v>0,[x'],\omega) = 0 \tag{27}$$

$$\tilde{k}_{10}(v>0,\omega) = 0 \tag{28}$$

$$S_r(v<0,[x'],\omega) = 0 \tag{29}$$

$$\tilde{k}_{13}(v<0,\omega) = 0 \tag{30}$$

(Remark: The operators $\mathcal{V}_{0l}$, $\mathcal{V}_{0r}$, $\mathcal{V}_l$, and $\mathcal{V}_r$ are not required here because the functions upon which they act vanish identically.)

D. The integral and coefficient equations

With the level-four quantities calculated in Subsec. III.C, we can now explicitly establish the integral equations (37)/I through (40)/I, as well as the equivalent matrix equation (48)/I, for the extended Pierce problem defined in Subsec. III.A.

Equation (37)/I remains unchanged:

$$Z_e(\omega)\,\tilde{j}_e(\omega) + \int_0^L dx'\,\tilde{E}(x',\omega) = -\tilde{V}_{e0}(\omega)\,. \tag{31}$$

However, due to the simple boundary conditions (7), Eq. (38)/I reduces to

$$-k_5(x,\omega)\,\tilde{j}_e(\omega) + \tilde{E}(x,\omega) = \tilde{k}_8(x,\omega)\,, \tag{32}$$

while Eqs. (39)/I and (40)/I are identically satisfied and hence need not be considered in what follows.

We thus have to solve Eqs. (31) and (32) for $\tilde{j}_e(\omega)$ and $\tilde{E}(x,\omega)$. The equivalent matrix equation for the expansion coefficients is given by Eq. (48)/I:

$$\underline{D}(\omega)\cdot\tilde{\mathbf{u}}(\omega)=\tilde{\mathbf{k}}(\omega)\,, \tag{33}$$

where the coefficient matrix $\underline{D}(\omega)$, the known-coefficient vector $\tilde{\mathbf{k}}(\omega)$, and the unknown-coefficient vector $\tilde{\mathbf{u}}(\omega)$ are now considerably reduced in comparison with their general counterparts (49a,b,c)/I:

$$\underline{D}(\omega)=\begin{pmatrix} Z_e & L\bar{\varphi}^T \\ -\mathbf{k}_5 & \underline{1} \end{pmatrix} \tag{34}$$

$$\tilde{\mathbf{k}}(\omega)=\begin{pmatrix} -\tilde{V}_{e0} \\ \tilde{\mathbf{k}}_8 \end{pmatrix} \qquad \tilde{\mathbf{u}}(\omega)=\begin{pmatrix} \tilde{j}_e \\ \tilde{\mathbf{E}} \end{pmatrix}. \tag{35a,b}$$

The determinant of (34) is easily found in the analytical form

$$\begin{aligned} |\underline{D}(\omega)| &= Z_e(\omega)+\sum_{\kappa'} k_5(\kappa',\omega)(L\bar{\varphi}_{\kappa'}) \\ &= Z_e(\omega)+\int_0^L dx\, k_5(x,\omega) \\ &= (\hat{R}-i\omega\hat{L})+\frac{4\pi i L}{\omega}R_3(\omega)\,. \end{aligned} \tag{36}$$

IV. SOLVING FOR THE BASIC MODES

A. Solution of the integral equations.

The solutions $\tilde{j}_e(\omega)$ and $\tilde{E}(x,\omega)$ to Eqs. (31) and (32) can be found analytically. On inserting $\tilde{E}(x,\omega)$, as calculated from (32), into (31), and taking into account (36), we readily obtain

$$\tilde{j}_e(\omega) = \frac{-\tilde{V}_{e0}(\omega) - \int_0^L dx\, \tilde{k}_8(x,\omega)}{|\underline{D}(\omega)|}\,. \tag{37}$$

Both the numerator and the denominator of this expression contain terms proportional to ω^{-1} and thus become singular for $\omega \to 0$. Since these singularities are inessential but inconvenient with respect to what follows, we multiply both the numerator and the denominator of (37) by ω. With a view to the basic modes defined in Subsec. III.B, we then re-write (37) in the form

$$\begin{aligned}\tilde{j}_e(\omega) &= \frac{\tilde{H}(\omega)}{G(\omega)} \\ &= \tilde{f}_{\xi i}\,\hat{j}_e^{(1)}(\omega|\xi) + \tilde{V}_{e\tau}\,\hat{j}_e^{(2)}(\omega|\tau) + \tilde{j}_{ei}\,\hat{j}_e^{(3)}(\omega) + \left(\frac{d\tilde{j}_e}{dt}\right)_i \hat{j}_e^{(4)}(\omega)\,,\end{aligned} \tag{38}$$

where

$$\begin{aligned}G(\omega) &\equiv \omega|\underline{D}(\omega)| \\ &= \omega\left(\hat{R} - i\omega\hat{L}\right) + 4\pi i L\, R_3(\omega)\,,\end{aligned} \tag{39}$$

$$\begin{aligned}\tilde{H}(\omega) &= \omega\left\{-\tilde{V}_{e0}(\omega) - \int_0^L dx\, \tilde{k}_8(x,\omega)\right\} \\ &= \tilde{f}_{\xi i}\,\hat{H}^{(1)}(\omega|\xi) + \tilde{V}_{e\tau}\,\hat{H}^{(2)}(\omega|\tau) + \tilde{j}_{ei}\,\hat{H}^{(3)}(\omega) + \left(\frac{d\tilde{j}_e}{dt}\right)_i \hat{H}^{(4)}(\omega)\,,\end{aligned} \tag{40}$$

$$\hat{H}^{(1)}(\omega|\xi) = -4\pi i e \left[(L-\xi)\, R_3(\omega) + L\frac{\omega}{\omega_p}\, R_4(\omega|\xi) \right] \tag{41a}$$

$$\hat{H}^{(2)}(\omega|\tau) = -\omega\, e^{i\omega\tau} \tag{41b}$$

$$\hat{H}^{(3)}(\omega) = \omega \hat{L} + i\hat{R}\, R_3(\omega) \tag{41c}$$

$$\hat{H}^{(4)}(\omega) = i\hat{L}\, R_3(\omega)\,, \tag{41d}$$

and

$$\hat{j}_e^{(1)}(\omega|\xi) = \frac{\hat{H}^{(1)}(\omega|\xi)}{G(\omega)} \tag{42a}$$

$$\hat{j}_e^{(2)}(\omega|\tau) = \frac{\hat{H}^{(2)}(\omega|\tau)}{G(\omega)} \tag{42b}$$

$$\hat{j}_e^{(3)}(\omega) = \frac{\hat{H}^{(3)}(\omega)}{G(\omega)} \tag{42c}$$

$$\hat{j}_e^{(4)}(\omega) = \frac{\hat{H}^{(4)}(\omega)}{G(\omega)}\,. \tag{42d}$$

Inserting (38) into (32) yields

$$\begin{aligned} \tilde{E}(x,\omega) &= \frac{\tilde{H}(\omega)}{G(\omega)} k_5(x,\omega) + \tilde{k}_8(x,\omega) \\ &= \tilde{f}_{\xi i}\, \hat{E}^{(1)}(x,\omega|\xi) + \tilde{V}_{e\tau}\, \hat{E}^{(2)}(x,\omega|\tau) \\ &+ \tilde{j}_{ei} \hat{E}^{(3)}(x,\omega) + \left(\frac{d\tilde{j}_e}{dt}\right)_i \hat{E}^{(4)}(x,\omega) \end{aligned} \tag{43}$$

where

$$\hat{E}^{(1)}(x,\omega|\xi) = \hat{j}_e^{(1)}(\omega|\xi)\, k_5(x,\omega) + \hat{k}_8^{(1)}(x,\omega|\xi) \tag{44a}$$

$$\hat{E}^{(2)}(x,\omega|\tau) = \hat{j}_e^{(2)}(\omega|\tau)\, k_5(x,\omega) \tag{44b}$$

$$\hat{E}^{(3)}(x,\omega) = \hat{j}_e^{(3)}(\omega)\, k_5(x,\omega) + \hat{k}_8^{(3)}(x,\omega) \tag{44c}$$

$$\hat{E}^{(4)}(x,\omega) = \hat{j}_e^{(4)}(\omega)\, k_5(x,\omega) + \hat{k}_8^{(4)}(x,\omega)\,. \tag{44d}$$

The functions $\hat{k}_8^{(1)}$ through $\hat{k}_8^{(4)}$ can be found in a straightforward manner by inspection of Eq. (26).

With (37) and (43) we have found the solutions to Eqs. (31) and (32), the time Laplace transforms of the basic modes being given by Eqs. (42) and (44).

B. Inverse Laplace transformation and time-dependent basic modes

The Laplace transforms $\hat{j}_e^{(m)}(\omega)$ and $\hat{E}^{(m)}(x,\omega)$ $(m = 1,\ldots,4)$, as given by Eqs. (42) and (44), are explicit analytical functions of ω and can be easily inverted into the time-dependent basic modes $\hat{j}_e^{(m)}(t)$ and $\hat{E}^{(m)}(x,t)$, cf. Table I. Since in the present example the Laplace transforms exhibit no branch cuts, the inversion procedure requires the evaluation of pole contributions only, cf. Sec. II.G/I and Fig. 2/I. The poles to be considered are the plasma poles ($\omega = \pm\omega_p$) and the eigenfrequencies ($\omega = \omega_\nu$, $\nu = \ldots,1,2,\ldots$). According to Eqs. (60)/I and (39), the latter are the zeros of the determinant (36) or, equivalently, of the function $G(\omega)$:

$$G(\omega_\nu; L, \bar{v}, \bar{n}_p, \hat{R}, \hat{L}) = 0\,, \tag{45}$$

where all parameters are shown explicitly for later purposes.

After some algebra, application of the inverse time Laplace transformation (8b)/I to (42) and (44) leads to the time-dependent basic modes

$$\hat{j}_e^{(1)}(t|\xi) = \sum_\nu \frac{\hat{H}^{(1)}(\omega_\nu|\xi)}{i\,G'(\omega_\nu)}\, e^{-i\omega_\nu t} \tag{46a}$$

$$\begin{aligned}\hat{j}_e^{(2)}(t|\tau) &= U(t-\tau)\sum_\nu \frac{\hat{H}^{(2)}(\omega_\nu|\tau)}{i\,G'(\omega_\nu)}\, e^{-i\omega_\nu t} \\ &= U(t-\tau)\sum_\nu \frac{i\omega_\nu}{G'(\omega_\nu)}\, e^{-i\omega_\nu(t-\tau)}\end{aligned} \tag{46b}$$

$$\hat{j}_e^{(3)}(t) = \sum_\nu \frac{\hat{H}^{(3)}(\omega_\nu)}{i\,G'(\omega_\nu)}\, e^{-i\omega_\nu t} \tag{46c}$$

$$\hat{j}_e^{(4)}(t) = \sum_\nu \frac{\hat{H}^{(4)}(\omega_\nu)}{i\,G'(\omega_\nu)}\, e^{-i\omega_\nu t} \tag{46d}$$

and

$$\begin{aligned}\hat{E}^{(1)}(x,t|\xi) &= -4\pi e\, U\left(x - [\xi + \bar{v}t]\right) \cos\omega_p t \\ &+ U(x-\bar{v}t)\, 2\pi \sum_{\beta=\pm} \left\{ \left[e\left(1 - \frac{\xi}{L}\right) - \sum_\nu \frac{\hat{H}^{(1)}(\omega_\nu|\xi)}{(\omega_\nu + \beta\omega_p) G'(\omega_\nu)} \right] e^{i\beta\omega_p t} \right. \\ &\left. + \sum_\nu \frac{\hat{H}^{(1)}(\omega_\nu|\xi)}{G'(\omega_\nu)} \frac{e^{-i\omega_\nu t}}{\omega_\nu + \beta\omega_p} \right\} \\ &+ U(\bar{v}t - x) \sum_\nu \frac{4\pi}{\omega_\nu} \frac{\hat{H}^{(1)}(\omega_\nu|\xi)}{G'(\omega_\nu)} R_1(x,\omega_\nu)\, e^{-i\omega_\nu t}\end{aligned} \tag{47a}$$

$$\begin{aligned}\hat{E}^{(2)}(x,t|\tau) &= U(t-\tau)\, U\left(x - [t-\tau]\bar{v}\right) \sum_\nu \frac{2\pi\omega_\nu}{G'(\omega_\nu)} \sum_{\beta=\pm} \frac{e^{i\beta\omega_p(t-\tau)} - e^{-i\omega_\nu(t-\tau)}}{\omega_\nu + \beta\omega_p} \\ &+ U(t-\tau)\, U\left([t-\tau]\bar{v} - x\right) \left\{ \sum_\nu \frac{4\pi}{G'(\omega_\nu)} \cos\frac{\omega_p x}{\bar{v}} \right. \\ &\left. - \sum_\nu \frac{4\pi}{G'(\omega_\nu)} R_1(x,\omega_\nu)\, e^{-i\omega_\nu(t-\tau)} \right\}\end{aligned} \tag{47b}$$

$$\begin{aligned}\hat{E}^{(3)}(x,t) &= U(x-\bar{v}t) \left\{ -\sum_{\beta=\pm} \left[\sum_\nu \frac{2\pi\,\hat{H}^{(3)}(\omega_\nu)}{(\omega_\nu + \beta\omega_p) G'(\omega_\nu)} + \frac{\hat{R}}{2L} \right] e^{i\beta\omega_p t} \right. \\ &\left. + \sum_\nu \left[\sum_{\beta=\pm} \frac{2\pi}{\omega_\nu + \beta\omega_p} \right] \frac{\hat{H}^{(3)}(\omega_\nu)}{G'(\omega_\nu)}\, e^{-i\omega_\nu t} \right\} \\ &+ U(\bar{v}t - x) \sum_\nu \frac{4\pi\,\hat{H}^{(3)}(\omega_\nu)}{\omega_\nu\, G'(\omega_\nu)} R_1(x,\omega_\nu)\, e^{-i\omega_\nu t}\end{aligned} \tag{47c}$$

$$\hat{E}^{(4)}(x,t) = U(x-\bar{v}t)\left\{-\sum_{\beta=\pm}\left[\sum_{\nu}\frac{2\pi\,\hat{H}^{(4)}(\omega_\nu)}{(\omega_\nu+\beta\omega_p)\,G'(\omega_\nu)}+\frac{\hat{L}}{2L}\right]e^{i\beta\omega_p t}\right.$$

$$\left.+\sum_{\nu}\left[\sum_{\beta=\pm}\frac{2\pi}{\omega_\nu+\beta\omega_p}\right]\frac{\hat{H}^{(4)}(\omega_\nu)}{G'(\omega_\nu)}\,e^{-i\omega_\nu t}\right\} \qquad (47d)$$

$$+\,U(\bar{v}t-x)\sum_{\nu}\frac{4\pi\,\hat{H}^{(4)}(\omega_\nu)}{\omega_\nu\,G'(\omega_\nu)}\,R_1(x,\omega_\nu)\,e^{-i\omega_\nu t},$$

where $G' = dG/d\omega$. Since the asymptotic part in (47b) may not contain a constant term, we conclude that $\sum_\nu [G'(\omega_\nu)]^{-1} = 0$. From the basic modes (46) and (47), the general solution to our perturbational problem can be constructed as described in Subsec. III.B. For given initial perturbations and external-generator signals, this is a purely mechanical task which will not be pursued here any further. Let us recall that $\hat{j}_e^{(1)}$ and $\hat{E}^{(1)}$ are the spatial Green's functions (for initial plasma perturbations), and $\hat{j}_e^{(2)}$ and $\hat{E}^{(2)}$ are the temporal Green's functions (for external-generator signals).

By inspection of (46) we see that the external-circuit current densities $\tilde{j}_e^{(m)}(t)$ $(m = 1,\ldots,4)$ are just superpositions of exponentials $\exp(-i\omega_\nu t)$, i.e., their time behavior is exclusively governed by the eigenfrequencies ω_ν. While basic modes 1, 3, and 4 are due to initial perturbations and hence give non-zero contributions right from time $t = 0$ on, basic mode 2 is activated by an external delta pulse at time τ and hence contributes only for $t > \tau$.

According to (47), the corresponding electric-field patterns are much more complex in that each of them exhibits an initial transient and an asymptotic solution. At a given position x, the initial transient is on during the intervals $0 < t < x/\bar{v}$ (for basic modes 1,3,4) and $\tau < t < \tau + x/\bar{v}$ (for basic mode 2). Its time behavior is not only governed by the eigenfrequencies but also by the

plasma frequency. The left-hand boundary of the transient pattern moves to the right as $x = \bar{v}t$ and $x = \bar{v}(t-\tau)$, respectively, thus giving way to the "clean" eigenmode pattern of the asymptotic solution. After $t = L/\bar{v}$ and $t = \tau + L/\bar{v}$, respectively, the transient is no longer present, and only eigenmodes are left in the system. Inspection of (47a–d) shows that the electric-field profile associated with an eigenfrequency ω_ν is essentially given by the function $R_1(x, \omega_\nu)$ as defined by (12a).

After a sufficiently long time, the "uppermost" eigenmode—i.e., the one with the most positive $\mathrm{Im}\,\omega_\nu$—will be dominant.

V. CHARACTERISTIC EQUATION, EIGENFREQUENCIES, AND EIGENMODES

With the basic-mode solutions (46) and (47), the detailed linear evolution of our Pierce-type diode can be calculated for arbitrary initial and external perturbations (9), (10) as indicated by Eq. (11). The full details of this evolution may be required, e.g., for interpreting an experiment where the propagation of externally generated small-amplitude pulses is studied. In many applications, however, it will be sufficient to concentrate on the asymptotic behavior. Whichever is the case, the evaluation of Eqs. (46) and (47) requires quantitative determination of the eigenfrequencies ω_ν. These and the associated eigenmode profiles are the subject of the present section.

A. Normalized characteristic equation

Quite discouragingly, the eigenfrequencies ω_ν are functions of no less than five physical parameters, namely of the quantities L, $\bar{v}$, $\bar{n}_p$, $\hat{R}$, and $\hat{L}$ appearing in the characteristic equation, or "dispersion relation", (45). However, the complexity of the problem can be substantially reduced by introducing appropriate normalizations. Let us re-write Eq. (45) in the nondimensional form

$$\hat{G}(\eta_\nu; \alpha, \rho, \lambda) = 0 \tag{48}$$

where

$$\eta = \frac{\omega}{\omega_p} \tag{49}$$

is the normalized frequency, α is the classical Pierce parameter defined by Eq. (1),

$$\rho = \frac{\hat{R}\omega_p^2}{4\pi\bar{v}} \tag{50a}$$

$$\lambda = \frac{\hat{L}\omega_p^3}{4\pi\bar{v}} \tag{50b}$$

are the normalized external-circuit resistance and inductance, respectively, and

$$\begin{aligned}\hat{G}(\eta;\alpha,\rho,\lambda) &\equiv \frac{\omega_p\, G(\omega)}{4\pi i\bar{v}} \\ &= (\eta^2-1)^{-2}\left\{e^{i\alpha\eta}\left[(\eta^2+1)\sin\alpha + 2i\eta\cos\alpha\right]\right. \\ &\left. -\lambda\eta^6 - i\rho\eta^5 + (\alpha+2\lambda)\eta^4 + 2i\rho\eta^3 - (\alpha+\lambda)\eta^2 - i(2+\rho)\eta\right\}.\end{aligned} \tag{51}$$

We thus have to solve for the roots η_ν of Eq. (48), which are the normalized eigenfrequencies and "only" depend on the three parameters α, ρ, and λ. Each of these parameters may vary between 0 and ∞, and for each parameter triple there are infinitely many eigenfrequencies η_ν, whose imaginary parts are bounded from above. The question thus arises of how to investigate in a systematic manner the relevant eigenfrequencies and the associated eigenmode profiles in a given parameter domain of interest.

B. Eigenfrequencies

For a given parameter triple (α,ρ,λ), all eigenfrequencies down to some chosen $(\mathrm{Im}\,\eta)_{min}$ can be approximately located as follows. One starts out by plotting the complex image curves $\hat{G}(\eta;\alpha,\rho,\lambda)$ for a suitable sequence of complex straight-line portions of the form $(-M \le \mathrm{Re}\,\eta \le M, \mathrm{Im}\,\eta = \text{const.})$, where M is positive and sufficiently large to simulate infinity, and $\mathrm{Im}\,\eta$ assumes successively lower values from some suitable $(\mathrm{Im}\,\eta)_{max}$ down to $(\mathrm{Im}\,\eta)_{min}$. By inspection of the image curves one has to find out which ones come close to the origin $\hat{G}=0$, and at which values of $\mathrm{Re}\,\eta$. One thus obtains the starting values

needed for the numerical solution of Eq. (48). This procedure is closely related to the classical Nyquist method[53] and can, in principle, be automated.

Due to the symmetry

$$\hat{G}(-\operatorname{Re}\eta + i\operatorname{Im}\eta;\alpha,\rho,\lambda) = \left[\hat{G}(+\operatorname{Re}\eta + i\operatorname{Im}\eta;\alpha,\rho,\lambda)\right]^{*}, \qquad (52)$$

which is not difficult to verify on Eq. (51), we have that eigenfrequencies with a non-vanishing real part always occur in pairs of the form

$$\eta_{\mu\pm}^{(d)} = \pm\operatorname{Re}\eta_{\mu}^{(d)} + i\operatorname{Im}\eta_{\mu}^{(d)}, \qquad (53)$$

where the superscript (d) indicates the "doublet" character of these eigenfrequencies, and $\operatorname{Re}\eta_{\mu}^{(d)}$ is defined to be positive. Similarly, we will label purely imaginary, or "singlet", roots of Eq. (48) by the superscript (s).

As will become apparent in the following subsection, both eigenfrequencies of a doublet (53) correspond to one and the same eigenmode, so that it is convenient to distinguish between the "eigenfrequency index" ν and the "eigenmode index" μ. Thus, a doublet (53) corresponds to two values of ν but to just one value of μ.

C. Eigenmode profiles

By inspecting the asymptotic parts of the basic-mode solutions (47a–d) we see that the complex electric field associated with an eigenfrequency $\omega_\nu \equiv \omega_p\eta_\nu$ is generally given by

$$E_{\nu}^{(c)}(x,t) = C\,R_1(x,\omega_\nu)\,e^{-i(\omega_\nu t+\gamma)} \qquad (54)$$

with C and γ real. This equation can be re-written in the form

$$
\begin{aligned}
E_\nu^{(c)}(x,t) = C\,\{&\mathrm{Re}\,R_1(x,\omega_\nu)\,\cos(\mathrm{Re}\,\omega_\nu t+\gamma)\\
&+\mathrm{Im}\,R_1(x,\omega_\nu)\,\sin(\mathrm{Re}\,\omega_\nu t+\gamma)\}\;e^{\mathrm{Im}\,\omega_\nu t}\\
+iC\,\Big\{&\mathrm{Re}\,R_1(x,\omega_\nu)\,\cos(\mathrm{Re}\,\omega_\nu t+\gamma+\frac{\pi}{2})\\
&+\mathrm{Im}\,R_1(x,\omega_\nu)\,\sin(\mathrm{Re}\,\omega_\nu t+\gamma+\frac{\pi}{2})\Big\}\;e^{\mathrm{Im}\,\omega_\nu t}\,,
\end{aligned}
\tag{55}
$$

from which it is evident that the real and imaginary parts describe the same spatial and temporal behavior, except for an amplitude factor i and a phase difference $\pi/2$. Hence, we may, without loss of generality, define a real and normalized eigenmode profile by the real part of Eq. (55), with $C = 1$ and $\gamma = 0$:

$$
\begin{aligned}
E_\nu^{(rn)} = \{&\mathrm{Re}\,R_1(x,\omega_\nu)\,\cos(\mathrm{Re}\,\omega_\nu t)\\
&+\mathrm{Im}\,R_1(x,\omega_\nu)\,\sin(\mathrm{Re}\,\omega_\nu t)\}\;e^{\mathrm{Im}\,\omega_\nu t}
\end{aligned}
\tag{56}
$$

We furthermore choose to define the associated potential profile in the normalized form

$$
\begin{aligned}
V_\nu^{(rn)}(x,t) &= -\frac{1}{L}\int_0^x dx'\,E_\nu^{(rn)}(x',t)\\
&= \{Re R_5(x,\omega_\nu)\,\cos(\mathrm{Re}\,\omega_\nu t)+\mathrm{Im}\,R_5(x,\omega_\nu)\,\sin(\mathrm{Re}\,\omega_\nu t)\}\;e^{\mathrm{Im}\,\omega_\nu t}\,.
\end{aligned}
\tag{57}
$$

Since the functions $R_1(x,\omega)$ and $R_5(x,\omega)$ exhibit the symmetry

$$
R_{1,5}(x,-\mathrm{Re}\,\omega+i\,\mathrm{Im}\,\omega) = [R_{1,5}(x,+\mathrm{Re}\,\omega+i\,\mathrm{Im}\,\omega)]^*\,, \tag{58}
$$

Eqs. (56) and (57) imply

$$
E_{\mu+}^{(rn)}(x,t) = E_{\mu-}^{(rn)}(x,t) = E_\mu^{(rn)}(x,t) \tag{59a}
$$

$$
V_{\mu+}^{(rn)}(x,t) = V_{\mu-}^{(rn)}(x,t) = V_\mu^{(rn)}(x,t)\,, \tag{59b}
$$

so that both eigenfrequencies of a doublet (53) correspond to one and the same physical eigenmode.

Clearly, $\mathrm{Re}\, R_1(x,\omega_\nu)$ and $\mathrm{Re}\, R_5(x,\omega_\nu)$ represent the initial values of the eigenmode profiles (56) and (57), respectively. One easily verifies that $\mathrm{Re}\, R_1(0,\omega_\nu) = 1$ and $\mathrm{Im}\, R_1(0,\omega_\nu) = \mathrm{Re}\, R_5(0,\omega_\nu) = \mathrm{Im}\, R_5(0,\omega_\nu) = 0$. Since the constant-emission assumption (7a) implies zero space-charge perturbation at $x = x_l \to 0$, we also expect $\partial(\mathrm{Re}\, R_1)/\partial x = \partial(\mathrm{Im}\, R_1)/\partial x = 0$ for $x \to 0$. For a singlet eigenfrequency ($\mathrm{Re}\,\omega_\mu^{(s)} = 0$), both $\mathrm{Im}\, R_1$ and $\mathrm{Im}\, R_5$ vanish identically, and the eigenmodes are either purely damped ($\mathrm{Im}\,\omega_\mu^{(s)} < 0$) or purely growing ($\mathrm{Im}\,\omega_\mu^{(s)} > 0$), thus retaining their initial spatial profiles. (We have not investigated the details of the singular case $\omega_\mu = 0$.) For doublet eigenfrequencies ($\mathrm{Re}\,\omega_\mu^{(d)} \neq 0$), $\mathrm{Im}\, R_1(x,\omega_\mu^{(d)})$ and $\mathrm{Im}\, R_5(x,\omega_\mu^{(d)})$ represent the spatial field and potential structures after a quarter-period, $\mathrm{Re}\,\omega_\mu^{(d)} t = \pi/2$, and the eigenmode is a superposition of two damped ($\mathrm{Im}\,\omega_\mu^{(d)} < 0$), constant-amplitude ($\mathrm{Im}\,\omega_\mu^{(d)} = 0$), or growing ($\mathrm{Im}\,\omega_\mu^{(d)} > 0$) standing waves with different spatial profiles and a temporal phase difference of $\frac{\pi}{2}$, respectively resulting in a damped, constant-amplitude, or growing propagating-wave-like structure.

In view of the foregoing remarks, the spatial field and potential structures of an eigenmode corresponding to a singlet eigenfrequency $\omega_\mu^{(s)}$ are uniquely represented by $\mathrm{Re}\, R_1(x,\omega_\mu^{(s)})$ and $\mathrm{Re}\, R_5(x,\omega_\mu^{(s)})$, respectively. Representation of a doublet eigenmode, on the other hand, in addition requires the functions $\mathrm{Im}\, R_1(x,\omega_\mu^{(d)})$ and $\mathrm{Im}\, R_5(x,\omega_\mu^{(d)})$.

VI. NUMERICAL RESULTS

In this section we present systematic numerical results for the uppermost normalized eigenfrequencies and the associated eigenmode profiles in some typical parameter domains, cf. Sec. V. In Subsec. VI.A., the classical, short-circuited Pierce diode, which lends itself as a convenient standard case, is reviewed, a classification scheme for the eigenfrequencies is introduced, and some new eigenfrequencies are calculated. The effects of external-circuit resistance and external-circuit inductance on the eigenfrequencies and eigenmode profiles are considered in Subsecs. VI.B and VI.C, respectively. Some general aspects and implications are discussed in Subsec. VI.D.

A. The classical, short-circuited Pierce diode ($\alpha > 0, \rho = 0, \lambda = 0$)

The classical Pierce diode,[3] defined in Subsec. II.A, offers itself as a reference case to which all modified configurations can be conveniently compared. Numerical results for the dominant eigenfrequencies have been given before,[33,34] but for the systematic description attempted here we have found it necessary to complement these, in the parameter domains considered, with new results for some of the lower (with respect to $\mathrm{Im}\,\eta$) eigenfrequencies. Moreover, since only little information on eigenmode structures can be found in the literature,[13,17] we present, throughout this section, some typical eigenmode profiles. Following Subsec. V.C, these are represented in terms of the functions $\mathrm{Re}\,R_1$, $\mathrm{Im}\,R_1$, ReR_5, and $\mathrm{Im}\,R_5$.

Throughout the present section, we restrict ourselves to varying the Pierce parameter in the range $0.16\pi \leq \alpha \leq 3\pi$, for which the uppermost eigenfrequencies are shown in Fig. 4. This range is representative in that it covers

the "archetypical" α-intervals $0 < \alpha < \pi$, $\pi < \alpha < 2\pi$, and $2\pi < \alpha < 3\pi$, which will be seen to exhibit all possible modes of linear behavior. Since these three intervals are distinctly different from each other, it is convenient to number the eigenfrequencies uniformly within each of them. For a given α-interval $n\pi < \alpha < (n+1)\pi$, where $n = 0, 1, 2, \ldots$, we choose to number the eigenfrequencies η_μ so as to reflect the ordering of $\mathrm{Im}\,\eta_\mu$ in the middle of the interval, i.e., at $\alpha = (n + \frac{1}{2})\pi$. Thus, the eigenfrequency singlet or doublet with the uppermost imaginary part there is assigned $\mu = 1$ throughout the interval, the singlet or doublet with the next lower imaginary part there is assigned $\mu = 2$ throughout the interval, etc. If $\mu = 2$ corresponds to say an eigenfrequency doublet, we will speak of "eigenmode $2^{(d)}$", etc.

Throughout the three α-intervals shown in Fig. 4, the ordering of the eigenfrequencies $2^{(d)}$ and $3^{(d)}$ remains the same, so that no re-numbering is necessary at the transition between intervals. Above $3^{(d)}$, there exist no other eigenfrequencies than the ones shown. With increasing α, the packing density of the eigenfrequencies with respect to $\mathrm{Im}\,\eta$ increases rapidly. Thus, at $\alpha = 0.5\pi = 1.5708$ there are only five eigenfrequencies with $\mathrm{Im}\,\eta \geq -3.5$ (a doublet counts for two eigenfrequencies), at $\alpha = 1.5\pi = 4.7124$ there are six eigenfrequencies with $\mathrm{Im}\,\eta \geq -1$, whereas at $\alpha = 2.5\pi = 7.8540$ we already find 44 eigenfrequencies with $\mathrm{Im}\,\eta \geq -1$. Eigenfrequencies lying below $3^{(d)}$ are not shown, with the exception of the singlets $4^{(s)}$ (in $\pi < \alpha < 2\pi$) and $\mathrm{X}^{(s)}$ (in $2\pi < \alpha < 3\pi$; order μ unknown).

Figure 4 shows that the dominant eigenmodes ($\mu = 1$), which determine the linear time-asymptotic behavior, are non-oscillatory stable, or purely damped, for $0 < \alpha < \pi$, non-oscillatory unstable, or purely growing, for $\pi < \alpha < 2\pi$,

oscillatory unstable for $2\pi < \alpha < 3\pi - \epsilon$ (where $\epsilon \simeq 0.3$), and both oscillatory and non-oscillatory stable for $3\pi - \epsilon < \alpha < 3\pi$. The pattern of the last two intervals basically repeats with increasing α, so that for $3\pi < \alpha < 4\pi$ we have non-oscillatory instability, etc.; for large values of α, the growth rates decrease approximately as α^{-1}.[33,34]

Electric-field and electric-potential profiles of the dominant eigenmodes for $\alpha = 0.5\pi$, 1.5π, and 2.5π are shown in Figs. 6 and 12, Figs. 8 and 14, and Figs. 10 and 16, respectively. For the classical case, the field and potential structures become more complex with increasing α, and the potential profiles always return to zero at $x = L$.

B. The purely resistive case ($\alpha > 0, \rho > 0, \lambda = 0$)

The purpose of the present subsection is to establish how the eigenfrequencies and eigenmode structures change if we allow for finite resistance, but still require zero inductance, in the external circuit. We decide to answer this question for the three α-values 1.5π, 1.5π, and 2.5π, as representatives of the α-intervals they are located in, cf. Subsec. VI.A. For each α, the imaginary and real parts of the normalized eigenfrequencies η_μ are plotted for normalized resistances in the range $0 \leq \rho \leq 100$, and some typical field and potential profiles are given for the dominant eigenmodes. The value $\rho = 0$ retrieves the classical short-circuit case, while $\rho \to \infty$ corresponds to the open-circuit, or floating, diode.

Fig. 5 shows the eigenfrequencies $\eta_1^{(s)}$, $\eta_2^{(d)}$, and $\eta_3^{(d)}$ for $\alpha = 0.5\pi$. No other eigenfrequencies were found above $3^{(d)}$. We observe that increasing resistance results in weaker damping for $1^{(s)}$ but stronger damping for $2^{(d)}$ and $3^{(d)}$. Thus,

the system becomes "less stable" with increasing resistance, and tends towards marginal stability for large ρ. Figure 6 shows that the eigenmode profiles of $1^{(d)}$ change significantly with ρ.

The eigenfrequencies $\eta_1^{(s)}$, $\eta_2^{(d)}$, $\eta_3^{(d)}$, and $\eta_4^{(s)}$ for $\alpha = 1.5\pi$ are shown in Fig. 7. No other eigenfrequencies were found above $4^{(s)}$ and $3^{(d)}$, respectively. The most remarkable result is that $1^{(s)}$ remains unstable. However, $\mathrm{Im}\,\eta_1^{(s)}$ decreases monotonically with increasing ρ, and the system approaches marginal stability as $\rho \to \infty$. Figure 7 also shows that $\mathrm{Im}\,\eta_4^{(s)}$ crosses $\mathrm{Im}\,\eta_3^{(d)}$ at $\rho \simeq 3$, so that from there on $4^{(s)}$ is the third highest mode. Profiles of eigenmode $1^{(s)}$ for different values of ρ are given in Fig. 8.

Figure 9 shows the eigenfrequencies of the modes $1^{(d)}$, $2^{(d)}$, $3^{(d)}$, $\mathrm{X}^{(s)}$, $X^{(s)\prime}$, and $X^{(s)\prime\prime}$ for $\alpha = 2.5\pi$. No other eigenfrequencies were found above $3^{(d)}$. Here we encounter a much more complex and interesting behavior than for $\alpha = 0.5\pi$ (Fig. 5) and $\alpha = 1.5\pi$ (Fig. 7). The classically unstable mode $1^{(d)}$ is stabilized at $\rho \simeq 4$. At $\rho \simeq 19.2$, $\eta_1^{(d)}$ is "absorbed" by a singlet mode, which is seen to be the continuation of the classically high-order mode $\mathrm{X}^{(s)}$, cf. Fig. 4. Quite strangely, the imaginary part of $\eta_X^{(s)}$ describes an S-shaped curve which, for $19.2 \lesssim \rho \lesssim 93$, exhibits three branches denoted by $\mathrm{X}^{(s)}$, $X^{(s)\prime}$, and $X^{(s)\prime\prime}$. At $\rho \simeq 93$, a doublet branches off to the right, which we interpret as the continuation of $1^{(d)}$. Returning to the uppermost eigenfrequencies we may state that the dominating eigenmode is oscillatory growing for $0 \leq \rho \lesssim 4$, oscillatory damped for $4 \lesssim \rho \lesssim 19.2$, and purely damped for $\rho \gtrsim 19.2$. For large ρ, the system tends towards marginal instability. Eigenmode profiles of $1^{(d)}$ and $X^{(s)\prime\prime}$ for different values of ρ are given in Fig. 10.

C. The purely inductive case $(\alpha > 0, \rho = 0, \lambda > 0)$

In this subsection we investigate the eigenfrequencies and eigenmode structures for the case of finite inductance but zero resistance in the external circuit. As in Subsec. VI.B, we restrict ourselves to the three α-values 0.5π, 1.5π, and 2.5π. For each α, the uppermost eigenfrequencies are plotted in the range $0 \leq \lambda \leq 100$, and some typical eigenmode profiles are given. The value $\lambda = 0$ recovers the classical short-circuit case of Subsec. VI.A, whereas $\lambda \to \infty$ corresponds to a current-stabilized external circuit.

Fig. 11 shows the dependence on λ of the classical eigenfrequencies $\eta_1^{(s)}$, $\eta_2^{(d)}$, and $\eta_3^{(d)}$ for $\alpha = 0.5\pi$. However, we also observe a new doublet $L^{(d)}$ (eigenfrequency $\eta_L^{(d)}$), which does not exist for $\lambda = 0$ and thus is inherently due to the finite inductance in the external circuit. Since $\mathrm{Im}\,\eta_L^{(d)}$ always lies well above the imaginary parts of the other eigenfrequencies shown—no others were found above $3^{(d)}$ —the "inductive" mode $L^{(d)}$ is the dominant one and even goes unstable within some small intervals of the region $0 < \lambda \lesssim 0.09$. This means that the finite inductance now present has changed the linear response behavior fundamentally as compared with the short-circuit case, which is non-oscillatory stable. Fig. 12 shows some eigenmode profiles of $L^{(d)}$ for different values of λ. For $\lambda \to 0$, the oscillation frequency $\mathrm{Re}\,\eta_L^{(d)}$ tends towards infinity—which behavior is also observed for the other α-values considered—and thus precludes numerical solution of Eq. (48) for very small values of λ. As $\lambda \to \infty$, $\eta_L^{(d)}$ approaches zero, whereas the damping rates of the other modes increase logarithmically. With Eqs. (46a–d) in mind, this is the qualitative behavior we expect for the case of a current-stabilized external circuit.

The variation with λ of the eigenfrequencies $\eta_1^{(s)}$, $\eta_2^{(d)}$, $\eta_3^{(d)}$, $\eta_4^{(s)}$, and $\eta_L^{(d)}$ for $\alpha = 1.5\pi$ is shown in Fig. 13. No other modes were found above $3^{(d)}$. Contrary to $\alpha = 0.5\pi$, the classically dominant mode $1^{(s)}$ remains dominant, retaining its purely growing character. Its field and potential profiles change with λ as shown in Fig. 14. As $\lambda \to \infty$, both $\eta_1^{(s)}$ and $\eta_4^{(s)}$ tend to zero, whereas the damping rates of the other eigenfrequencies increase logarithmically. In some intervals of the region $\lambda \lesssim 1.1$, the inductive mode $L^{(d)}$ goes unstable.

Figure 15 shows the variation with λ of the eigenfrequencies $\eta_1^{(d)}$, $\eta_2^{(d)}$, $\eta_3^{(d)}$, and $\eta_L^{(d)}$ for $\alpha = 2.5\pi$. No other eigenfrequencies were found above $3^{(d)}$. The stability behavior is very similar to that for $\alpha = 1.5\pi$ (Fig. 13), except that now the dominant mode is an oscillatory one. Figure 16 shows the eigenmode profiles of $1^{(d)}$ for various values of λ. The inductive mode $L^{(d)}$ introduces additional instability within various intervals in the region $\lambda \lesssim 4$, at an oscillation frequency much higher than that of $1^{(d)}$.

D. Discussion

The results of the present section have shown that finite resistance or inductance in the external circuit can strongly modify the eigenfrequencies and eigenmode profiles as compared with their classical counterparts.

In Subsec. VI.B we have found that increasing the external-circuit resistance can change the dominant mode (i) from non-oscillatory stable to non-oscillatory marginally stable ($\alpha = 0.5\pi$), (ii) from non-oscillatory unstable to non-oscillatory marginally unstable ($\alpha = 1.5\pi$), and (iii) from oscillatory unstable successively to oscillatory stable, non-oscillatory stable, and non-oscillatory marginally stable ($\alpha = 2.5\pi$).

Perhaps the most interesting finding of this section is that finite external-circuit inductance gives rise to a new oscillatory mode $L^{(d)}$, which does not exist for $\lambda = 0$. The occurrence of this inductive mode is plausible because the system consisting of the diode, the resistance $\hat{R}$, and the inductance $\hat{L}$ (Fig. 1) may be looked upon as an *RLC* circuit, with the diode acting as a capacitor whose properties are partly determined by the plasma in it. Thus, the eigenmode $L^{(d)}$ may be interpreted as a modified *RLC* oscillation. For all values of α considered here, we have made the remarkable observation that there are regions of λ where $L^{(d)}$ is unstable, and that with increasing α these regions become larger. For $\alpha = 0.5\pi$, $L^{(d)}$ is the dominant mode, whereas for $\alpha = 1.5\pi$ and $\alpha = 2.5\pi$ it is second, at least in some range of λ.

Globally speaking, we have found that the linear response behavior of our Pierce-type diode depends crucially on all three parameters considered here, namely α, ρ, and λ. This induces us to speculate that also the nonlinear final states may strongly depend on these parameters, as well as on others that may have to be defined for more realistic cnfigurations. These final states can be time-independent, oscillatory, or turbulent,[34] and it appears that much more work is needed to clarify these phenomena, the parameter ranges in which they occur, and their dependencies on the parameters themselves. Particle simulations tackling some of these problems are under way and will be reported elsewhere.[43]

It should be borne in mind that the three cases considered in Subsecs. VI.A, VI.B, and VI.C are highly idealized ones, thus singling out specific external-circuit effects. Realistic external circuits, on the other hand, always involve resistive, inductive, and capacitive components in some more or less complex

combination, so that external-circuit effects may not always be as clear-cut as in the foregoing examples. Still, the above results are suitable to demonstrate that external circuits can matter quite substantially, and hence should be given proper consideration in every individual case.

VII. CONCLUSIONS

Using the method developped in Part I, we have given the complete analytical solution to the general linear perturbation problem for an extended Pierce-type diode. The configuration considered differs from the classical Pierce diode in that it exhibits a non-trivial external circuit involving a resistor, an inductor, and a signal generator.

Each of the solution functions given, $\tilde{j}_e(t)$ and $\tilde{E}(x,t)$, can be constructed by linear superposition of four different types of basic modes, namely a spatial Green's function associated with the initial perturbations of the plasma, a temporal Green's function accounting for external-generator signals, and two functions associated with the initial state of the external circuit. While $\tilde{j}_e$ always represents a sum of eigenoscillations only, $\tilde{E}(x,t)$ generally exhibits both an initial transient containing eigen- and plasma oscillations, and an asymptotic part made up of eigenmodes only.

After sufficiently long time, the linear dynamics is always dominated by the uppermost eigenmode. Hence, particular emphasis has been laid on presenting systematic numerical data covering the most important eigenfrequencies, as well as the associated eigenmode profiles, in some typical parameter domains. Among other things, it has been found that increasing external-circuit resistance can change an oscillatory unstable mode successively to oscillatory stable and non-oscillatory stable. Non-zero external-circuit inductance can create a new oscillatory mode, which may be dominant and even go unstable in parameter regions classically stable. Generally speaking, our results demonstrate that external circuits can, in fact, matter substantially and should, therefore, be properly accounted for in every individual case.

Apart from deriving these detailed results, we have also attempted to give a general account of the Pierce problem and its implications. In so doing it has been observed that the Pierce problem is potentially relevant to a wide class of laboratory plasmas and has recently been attracting a remarkable deal of interest in the context of various modern concepts and applications. More specifically, we have argued that the low-density single-ended Q machine can, to a certain extent, be approximated by a simple Pierce-type configuration.

In spite of the fairly large number of papers that have already been written on Pierce-type problems, we have to conclude that only rather restricted aspects have been studied so far, and that substantial progress in the theory of bounded plasma systems will require more comprehensive and realistic approaches. A first step in this direction has been proposed in Part I, but major extensions—e.g., to more general geometries—are still needed.

ACKNOWLEDGMENTS

The author is indebted to Prof. C. K. Birdsall, Dr. T. L. Crystal, and Prof. W. B. Thompson for valuable discussions. This work was supported in part by the U. S. Department of Energy under Contract DE-AT03-76ET53604, the U. S. Office of Naval Research under Contract N00014-77-C-0578, and the Austrian Fonds zur Förderung der wissenschaftlichen Forschung under Contract S-18/03. The computations were performed at the National Magnetic Fusion Energy Computing Center, Livermore.

References

[1]S. Kuhn, Part I of present work (to be published).

[2]Most of the concepts and symbols to be used in the present paper were already introduced in Part I, and references to the latter will be indicated by the suffix /I. Thus, Eq. (14) and Subsec. II.B of Part I are referred to as Eq. (14)/I and Subsec. II.B/I, respectively. Here, as in Part I, equilibrium quantities and perturbations are denoted by bar and tilde, respectively.

[3]J. R. Pierce, J. Appl. Phys. **15**, 721 (1944).

[4]J. R. Pierce, J. Appl. Phys. **21**, 1063 (1950).

[5]V. I. Volosov, Zh. Tekh. Fiz. **32**, 566 (1962) [Sov. Phys. Tech. Phys. **7**, 412 (1962)].

[6]M. N. Rosenbluth, L. D. Pearlstein, and G. W. Stuart, Phys. Fluids **6**, 1289 (1963).

[7]P. Burger, J. Appl. Phys. **35**, 3048 (1964).

[8]W. T. Norris, J. Appl. Phys. **35**, 3260 (1964).

[9]P. Burger, J. Appl. Phys. **36**, 1938 (1965).

[10]J. Frey and C. K. Birdsall, J. Appl. Phys. **36**, 2962 (1965).

[11]W. H. Cutler and P. Burger, J. Appl. Phys. **37**, 2867 (1966).

[12]H. Derfler and R. Holmstrom, J. Appl. Phys. **37**, 4189 (1966).

[13]J. Frey and C. K. Birdsall, J. Appl. Phys. **37**, 2051 (1966).

[14]V. M. Smirnov, Zh. Eksp. Teor. Fiz. **50**, 1005 (1966) [Sov. Phys. JETP **23**, 668 (1966)].

[15]P. Burger, J. Appl. Phys. **38**, 3360 (1967).

[16]V. D. Shapiro and V. I. Shevchenko, Zh. Eksper. Teor. Fiz. **52**, 142 (1967) [Sov. Phys. JETP **25**, 92 (1967)].

[17]J. E. Faulkner and A. A. Ware, J. Appl. Phys. **40**, 366 (1969).

[18]V. I. Kuznetsov and A. Ya. Ender, Zh. Tekh. Fiz. **42**, 2391 (1972) [Sov. Phys. Tech. Phys. **17**, 1859 (1973)].

[19]V. A. Buts, Zh. Tekh. Fiz. **44**, 1656 (1974) [Sov. Phys. Tech. Phys. **19**, 1034 (1975)].

[20]A. A. Ivanov and N. S. Putvinskaya, Zh. Tekh. Fiz. **45**, 1648 (1975) [Sov. Phys. Tech. Phys. **20**, 1049 (1976)].

[21]V. I. Kuznetsov and A. Ya. Ender, Zh. Tekh. Fiz. **47**, 2237 (1977) [Sov. Phys. Tech. Phys. **22**, 1295 (1977)].

[22]K. Saeki, S. Iizuka, N. Sato, and Y. Hatta, in *Proceedings of the Thirteenth International Conference on Phenomena in Ionized Gases, Berlin, German Democratic Republic, 1977* (VEB Buch-Export-Import, Leipzig, 1977), p. 783.

[23]K. Yuan, J. Appl. Phys. **48**, 133 (1977).

[24]G. Joyce and R. F. Hubbard, J. Plasma Phys. **20**, 391 (1978).

[25]V. A. Zherebtsov and V. D. Talanova, Zh. Tekh. Fiz. **48**, 349 (1978) [Sov. Phys. Tech. Phys. **23**, 207 (1978)].

[26]A. Ya. Ender and V. I. Kuznetsov, J. Physique (Paris), Colloque C7, supplément au n° 7, **40**, C7-523 (1979).

[27]S. Iizuka, K. Saeki, N. Sato, and Y. Hatta, Phys. Rev. Lett. **43**, 1404 (1979).

[28]V. I. Kuznetsov and A. Ya. Ender, Zh. Tekh. Fiz. **49**, 2176 (1979) [Sov. Phys. Tech. Phys. **24**, 1199 (1979)].

[29]V. I. Kuznetsov and A. Ya. Ender, Zh. Tekh. Fiz. **50**, 67 (1980) [Sov. Phys. Tech. Phys. **25**, 37 (1980)].

[30]J. W. Poukey, Report SAND80-2545, Sandia Laboratories, Albuquerque, NM 87185 (Nov. 1980).

[31]J. W. Poukey, J. P. Quintenz, and C. L. Olson, Appl. Phys. Lett. **38**, 21 (1981).

[32]J. W. Poukey, J. P. Quintenz, and C. L. Olson, J. Appl. Phys. **52**, 3016 (1981).

[33]J. R. Cary and D. S. Lemons, J. Appl. Phys. **53**, 3303 (1982).

[34]B. B. Godfrey, Reports AMRC-R-282 and AMRC-N-212, Mission Research Corp., Albuquerque, NM 87106 (April 1981 and November 1982, respectively).

[35]D. Jovanović, in *Proceedings of the Symposium on Plasma Double Layers, Risø National Laboratory, June 1982*, p. 90.

[36]S. Kuhn, in *Proceedings of the 1982 International Conference on Plasma Physics, Gøteborg, June 1982* (Chalmers University of Technology, Gøteborg, 1982), Contributed Papers, paper 11P-II-17.

[37]D. S. Lemons and J. R. Cary, J. Appl. Phys. **53**, 4093 (1982).

[38]R. A. Smith, Phys. Scripta **25**, 413 (1982).

[39]D. S. Lemons, Preprint LA-UR-82-1143, Los Alamos National Laboratory, Los Alamos, NM 87545 (1982).

[40]H. H. Atkinson, in *Proceedings of the Fourth International Congress on Microwave Tubes, Eindhoven 1963* (Centex Publishing Co., Eindhoven, 1963), p. 559.

[41]N. Sato, G. Popa, E. Märk, E. Mravlag, and R. Schrittwieser, Phys. Fluids **19**, 70 (1976).

[42]S. Iizuka, P. Michelsen, J. Juul Rasmussen, R. Schrittwieser, R. Hatakeyama, K. Saeki, and N. Sato, Phys. Rev. Lett. **48**, 145 (1982).

[43]C. K. Birdsall, T. L. Crystal, and S. Kuhn, to be published.

[44]R. G. McIntyre, J. Appl. Phys. **33**, 2485 (1962).

[45]I. G. Gverdtsiteli, V. A. Karakhanov, E. A. Kashirskii, R. Ya. Kucherov, and Z. A. Oganezov, Zh. Tekh. Fiz. **42**, 103 (1972) [Sov. Phys. Tech. Phys. **17**, 78 (1972)].

[46]W. Ott, Z. Naturforsch. **22a**, 1057 (1967).

[47]S. Kuhn, Plasma Phys. **21**, 613 (1979).

[48]S. Kuhn, Plasma Phys. **23**, 881 (1981).

[49]The present notation differs slightly from the one used in Refs. 47 and 48. The main differences are these: (i) The neutralization parameter, previously[47,48] called α, is now denoted by $\bar{\alpha}$. (ii) The bar accent, previously[47,48] used to denote averages, now indicates equilibrium quantities.

[50]G. Popa, M. Sanduloviciu, S. Kuhn, M. Oertl, and R. Schrittwieser, Phys. Lett. **87A**, 175 (1982).

[51]S. Kuhn, Phys. Rev. Lett. **50**, 217 (1983).

[52]S. Kuhn, A. D. R. Phelps, and M. T. C. Fang, Phys. Fluids **24**, 1586 (1981).

[53]N. A. Krall and A. W. Trivelpiece, *Principles of Plasma Physics* (McGraw-Hill, New York, 1973), p. 464.

Tables

TABLE I. Definition of basic modes.

basic mode no.	$\tilde{f}_{\xi i}$	$\tilde{V}_{e\tau}$	$\tilde{j}_{ei}$	$\left(\frac{d\tilde{j}_e}{dt}\right)_i$	$\tilde{j}_e(t)$	$\tilde{E}(x,t)$
1	1	0	0	0	$\hat{j}_e^{(1)}(t\|\xi)$	$\hat{E}^{(1)}(x,t\|\xi)$
2	0	1	0	0	$\hat{j}_e^{(2)}(t\|\tau)$	$\hat{E}^{(2)}(x,t\|\tau)$
3	0	0	1	0	$\hat{j}_e^{(3)}(t)$	$\hat{E}^{(3)}(x,t)$
4	0	0	0	1	$\hat{j}_e^{(4)}(t)$	$\hat{E}^{(4)}(x,t)$

Figure Captions

FIG. 1. Schematic of extended Pierce-type configuration.

FIG. 2. Pierce parameter over normalized system length versus neutralization parameter.

FIG. 3. Pierce parameter over system length versus equilibrium plasma density.

FIG. 4. Imaginary parts (a) and real parts (b) of the normalized eigenfrequencies $\eta_1^{(s)}$, $\eta_1^{(d)}$, $\eta_2^{(d)}$, $\eta_3^{(d)}$, $\eta_4^{(s)}$, and $\eta_X^{(s)}$ for $[0.16\pi \leq \alpha \leq 3\pi \,|\, \rho = 0 \,|\, \lambda = 0]$.

FIG. 5. Imaginary parts (a) and real parts (b) of the normalized eigenfrequencies $\eta_1^{(s)}$, $\eta_2^{(d)}$, and $\eta_3^{(d)}$ for $[\alpha = 0.5\pi \,|\, 0 \leq \rho \leq 100 \,|\, \lambda = 0]$.

FIG. 6. Electrostatic field (a) and potential (b) profiles of eigenmode $1^{(s)}$ for $[\alpha = 0.5\pi \,|\, \rho = 0, 1, 10, 100 \,|\, \lambda = 0]$.

FIG. 7. Imaginary parts (a) and real parts (b) of the normalized eigenfrequencies $\eta_1^{(s)}$, $\eta_2^{(d)}$, $\eta_3^{(d)}$, and $\eta_4^{(s)}$ for $[\alpha = 1.5\pi \,|\, 0 \leq \rho \leq 100 \,|\, \lambda = 0]$.

FIG. 8. Electrostatic field (a) and potential (b) profiles of eigenmode $1^{(s)}$ for $[\alpha = 1.5\pi \,|\, \rho = 0, 1, 10, 100 \,|\, \lambda = 0]$.

FIG. 9. Imaginary parts (a) and real parts (b) of the normalized eigenfrequencies $\eta_1^{(d)}$, $\eta_2^{(d)}$, $\eta_3^{(d)}$, $X^{(s)}$, $X^{(s)\prime}$, and $X^{(s)\prime\prime}$ for $[\alpha = 2.5\pi \,|\, 0 \leq \rho \leq 100 \,|\, \lambda = 0]$.

FIG. 10. Electrostatic field (a,b) and potential (c,d) profiles of eigenmode $1^{(d)}$ for $[\alpha = 2.5\pi \,|\, \rho = 0, 4, 19 \,|\, \lambda = 0]$, and of eigenmode $X^{(s)\prime\prime}$ for $[\alpha = 2.5\pi \,|\, \rho = 30, 100 \,|\, \lambda = 0]$.

FIG. 11. Imaginary parts (a) and real parts (b) of the normalized eigenfrequencies $\eta_1^{(s)}$, $\eta_2^{(d)}$, $\eta_3^{(d)}$, and $\eta_L^{(d)}$ for $[\alpha = 0.5\pi \,|\, \rho = 0 \,|\, 0 \leq \lambda \leq 100]$.

FIG. 12. Electrostatic field (a,b) and potential (c,d) profiles of eigenmode $L^{(d)}$ for $[\alpha = 0.5\pi \,|\, \rho = 0 \,|\, \lambda = 0.035, 0.07, 1, 10, 100]$.

FIG. 13. Imaginary parts (a) and real parts (b) of the normalized eigenfrequencies $\eta_1^{(s)}$, $\eta_2^{(d)}$, $\eta_3^{(d)}$, $\eta_4^{(s)}$, and $\eta_L^{(d)}$ for $[\alpha = 1.5\pi \,|\, \rho = 0 \,|\, 0 \leq \lambda \leq 100]$.

FIG. 14. Electrostatic field (a) and potential (b) profiles of eigenmode $1^{(s)}$ for $[\alpha = 1.5 \,|\, \rho = 0 \,|\, \lambda = 0, 1, 10, 100]$.

FIG. 15. Imaginary parts (a) and real parts (b) of the eigenfreqencies $\eta_1^{(d)}$, $\eta_2^{(d)}$, $\eta_3^{(d)}$, and $\eta_L^{(d)}$ for $[\alpha = 2.5\pi \,|\, \rho = 0 \,|\, 0 \leq \lambda \leq 100]$.

FIG. 16. Electrostatic field (a,b) and potential (c,d) profiles of eigenmode $1^{(d)}$ for $[\alpha = 2.5\pi \,|\, \rho = 0 \,|\, \lambda = 0, 1, 10, 100]$.

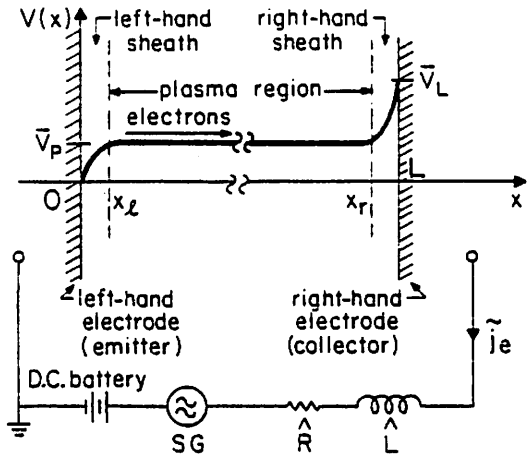

Fig. 1

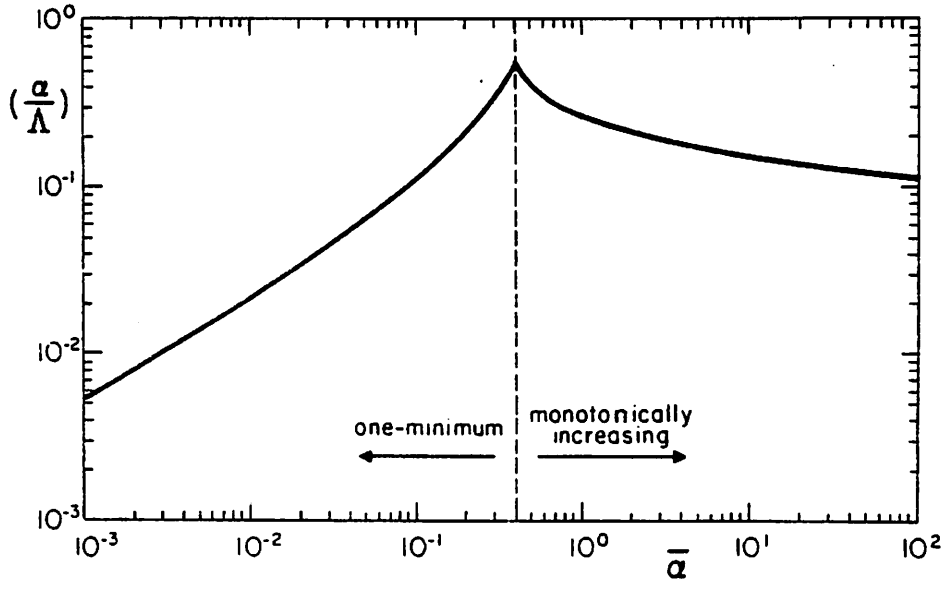

Fig. 2

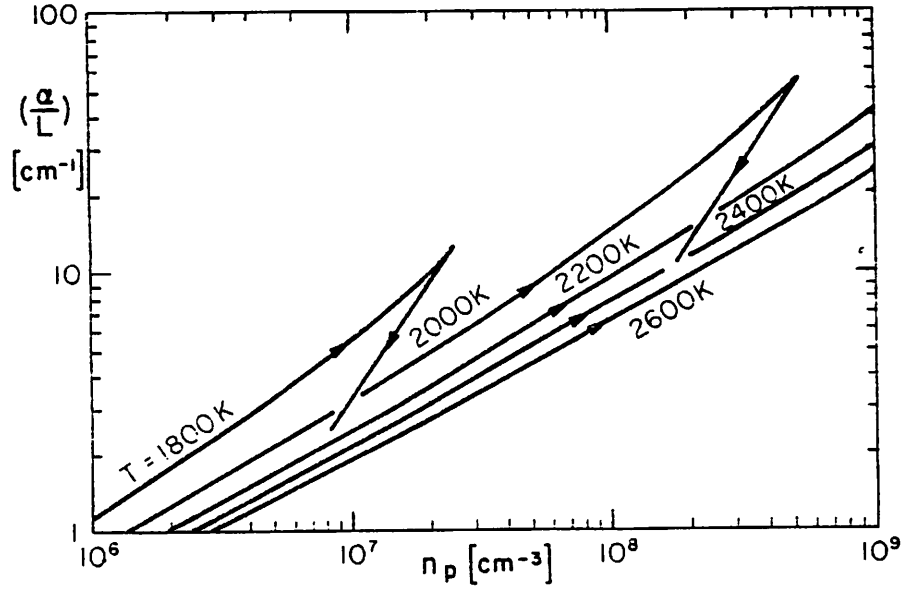

Fig. 3

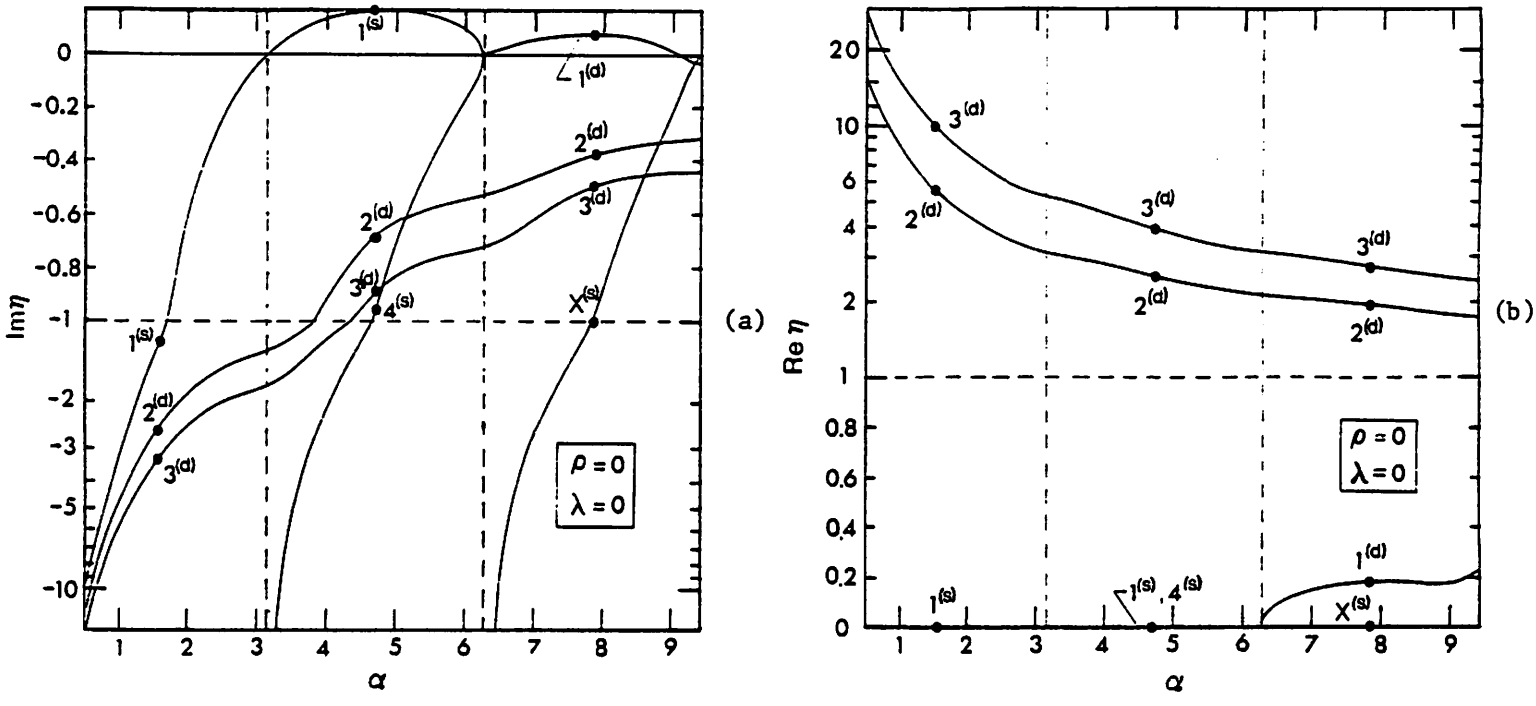

Fig. 4

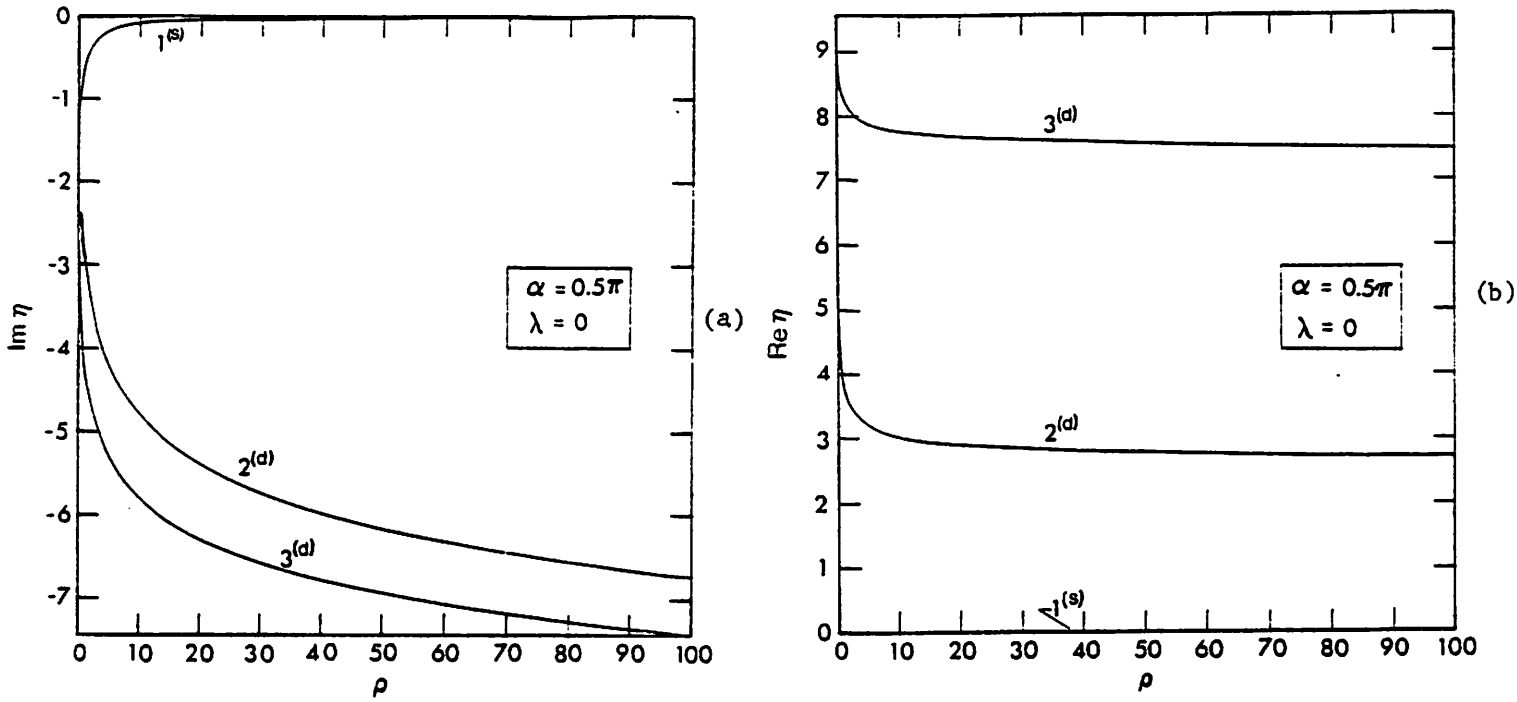

Fig. 5

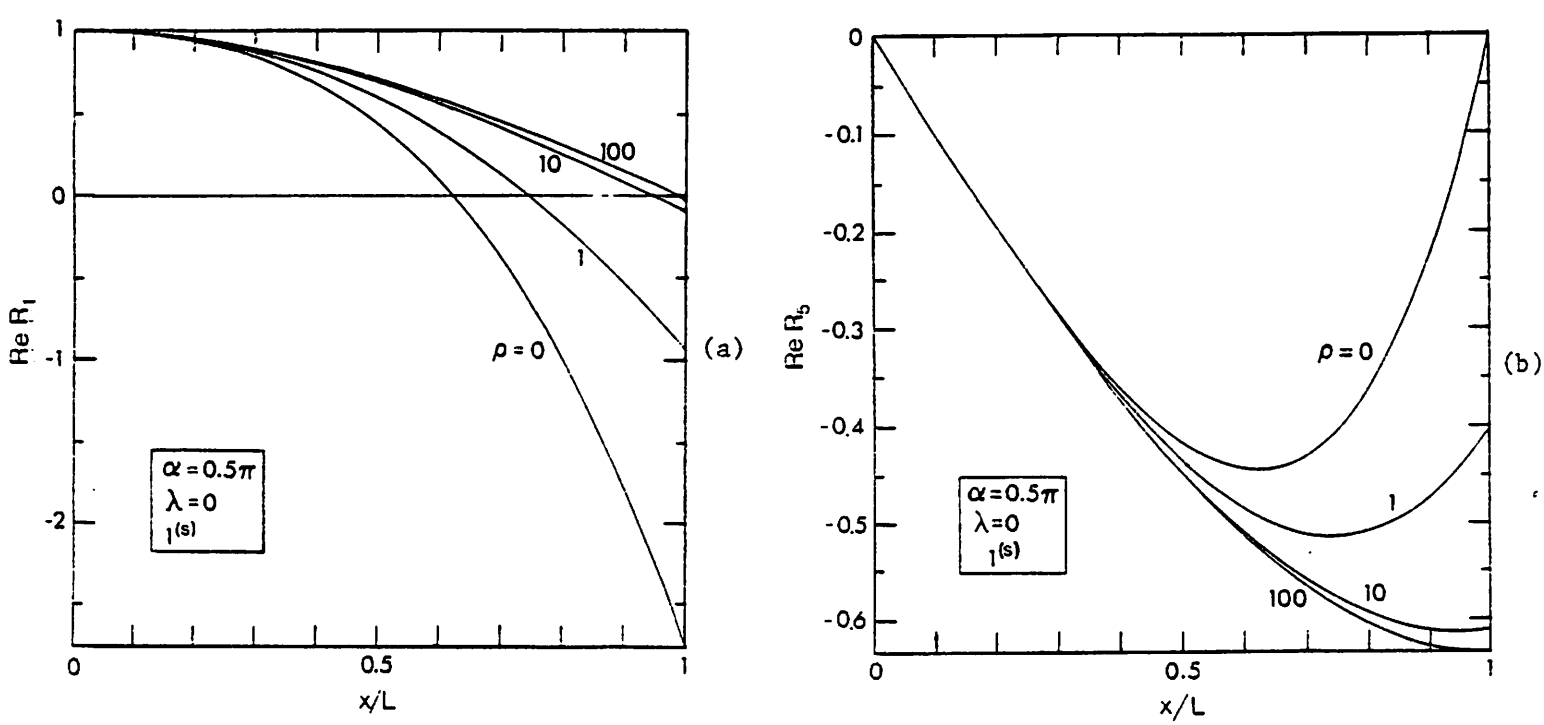

Fig. 6

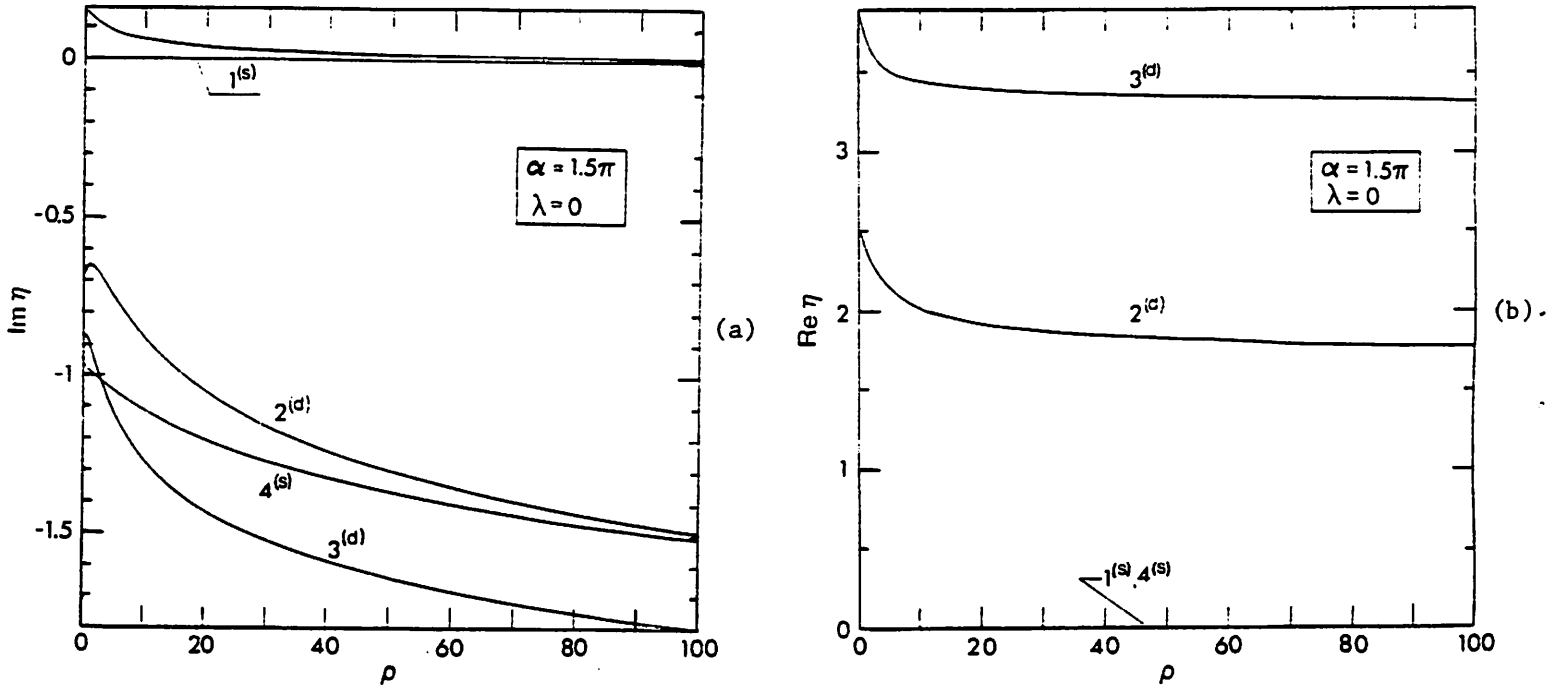
Im η
Re η
ρ
α = 1.5π
λ = 0
1(s)
2(d)
4(s)
3(d)
1(s), 4(s)
(a)
(b)

Fig. 7

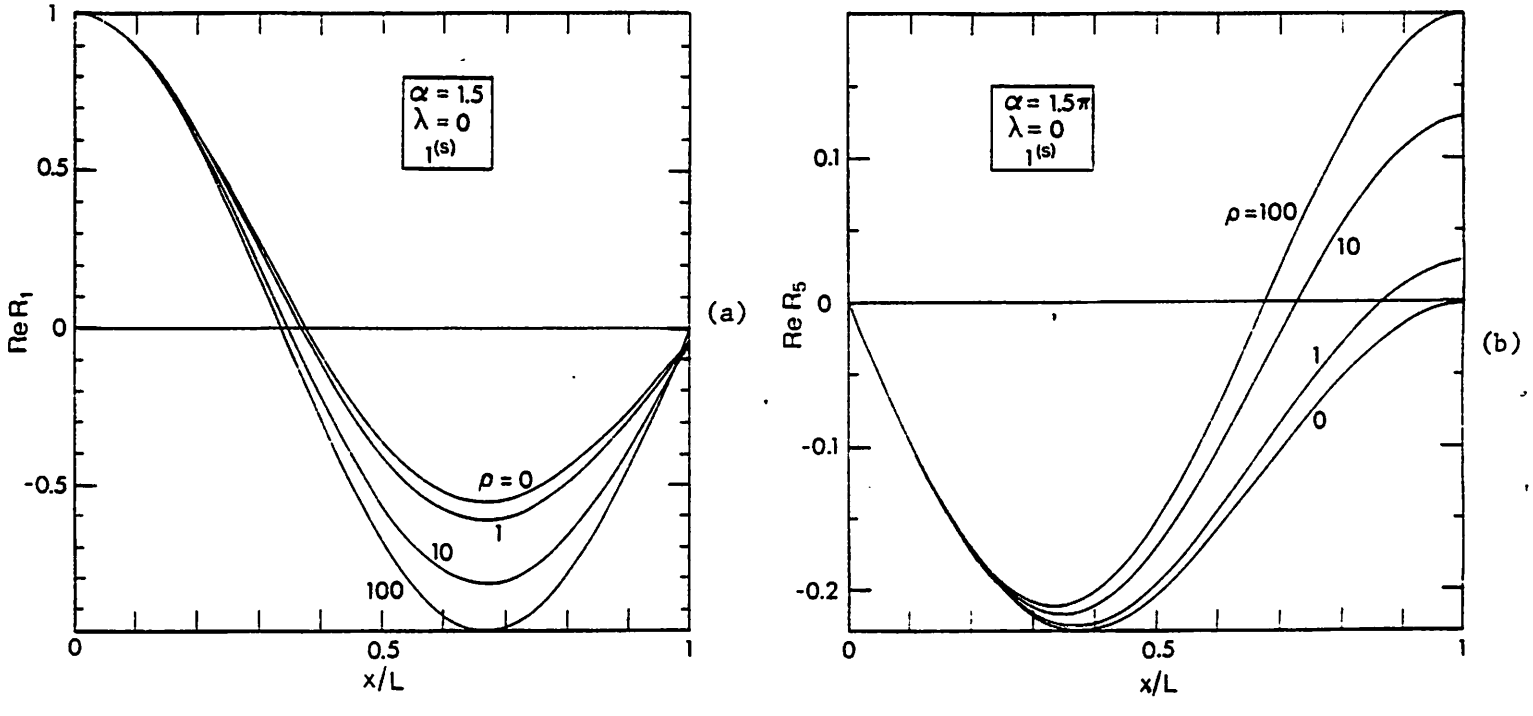
Re R1
Re R5
x/L
α = 1.5
α = 1.5π
λ = 0
1(s)
ρ = 0
1
10
100
ρ = 100
0
(a)
(b)

Fig. 8

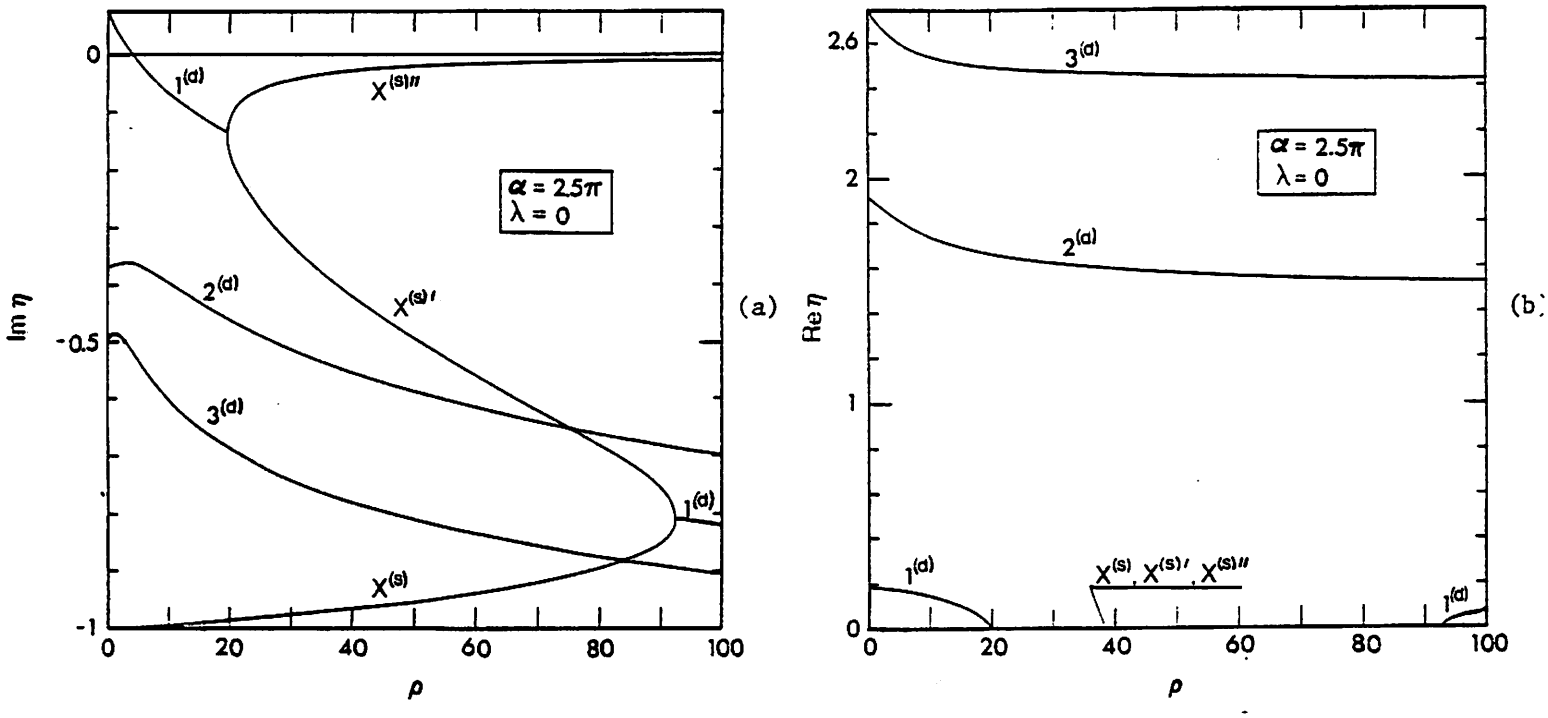
0
-0.5
-1
Im η
1(d)
X(s)II
α = 2.5π
λ = 0
2(d)
X(s)I
3(d)
1(d)
X(s)
0
20
40
60
80
100
ρ
(a)
2.6
2
1
0
Re η
3(d)
α = 2.5π
λ = 0
2(d)
1(d)
X(s), X(s)I, X(s)II
1(d)
0
20
40
60
80
100
ρ
(b)

Fig. 9

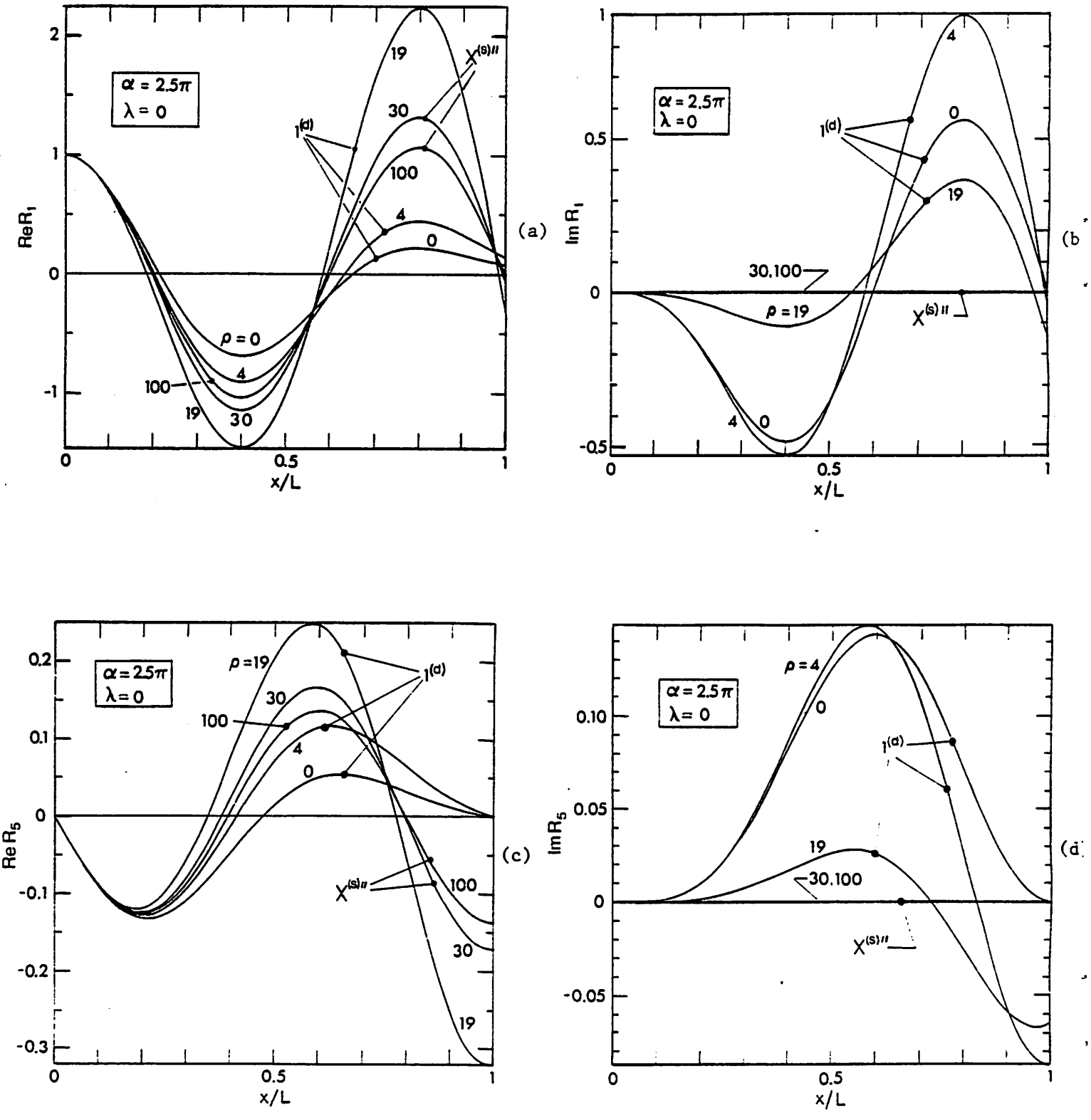
α = 2.5π
λ = 0
Re R1
x/L
ρ = 0
4
100
19
30
1(d)
X(s)II
(a)
Im R1
ρ = 19
30,100
0
(b)
Re R5
(c)
Im R5
ρ = 4
(d)

Fig. 10

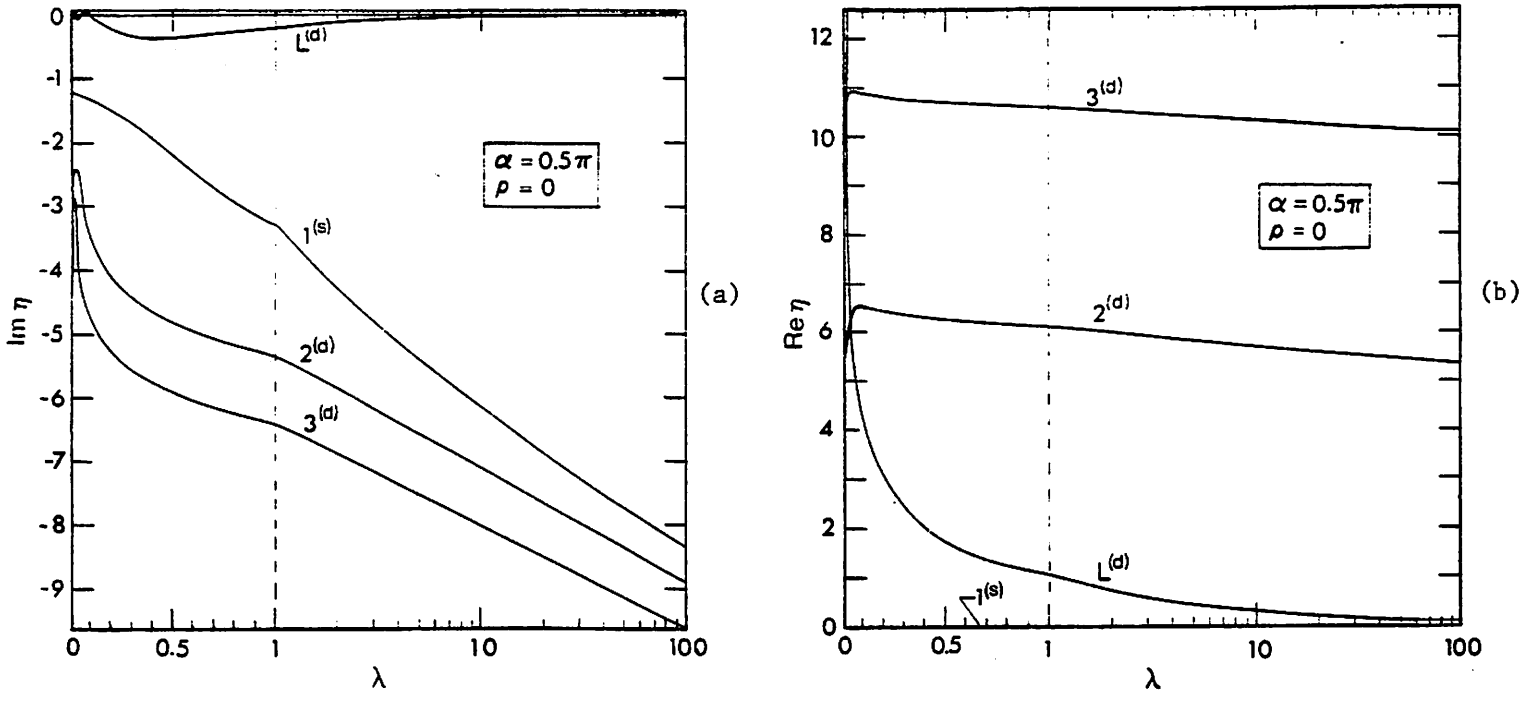

Fig. 11

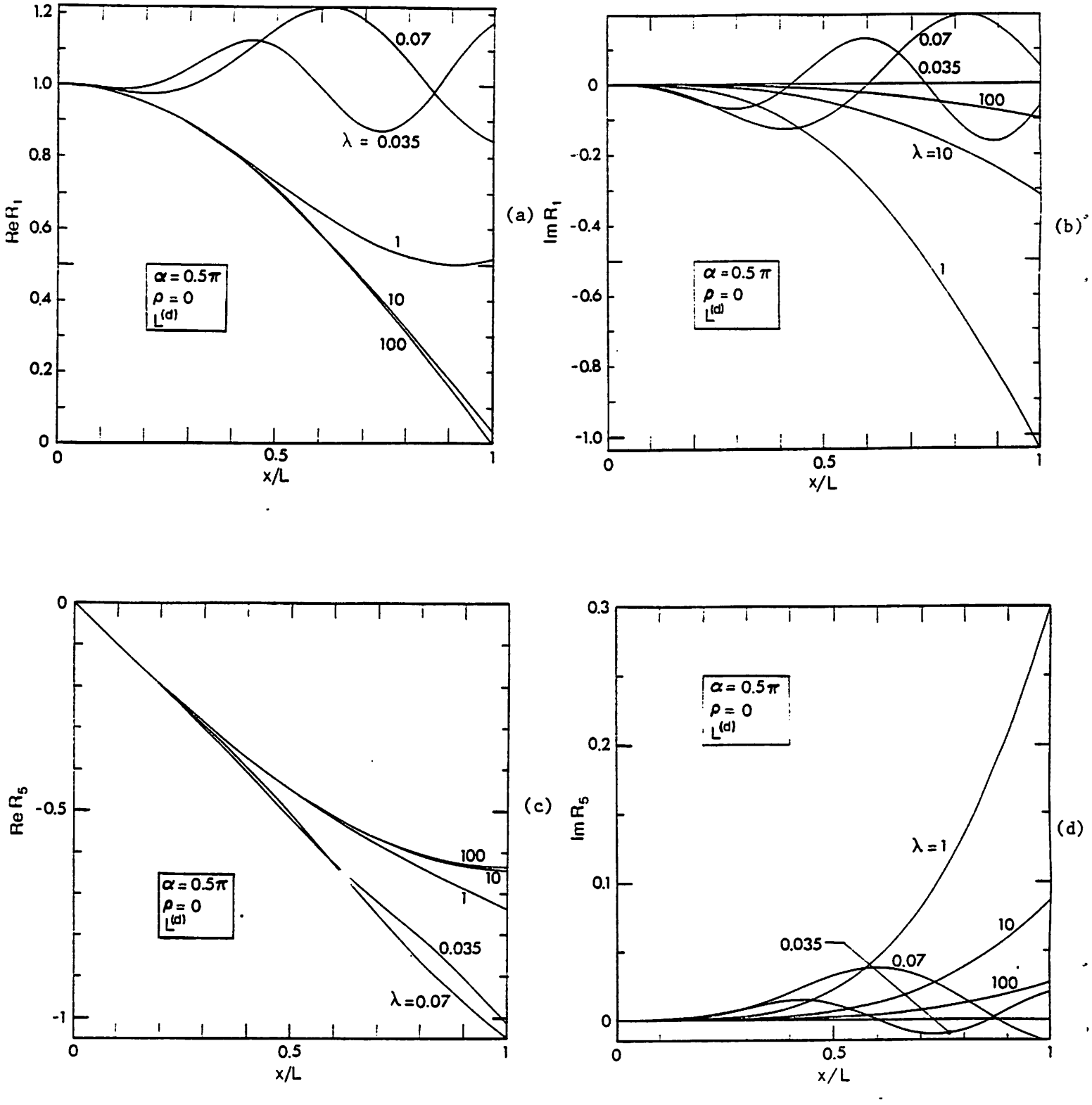
Re R1
x/L
α = 0.5π
ρ = 0
L(d)
0.07
λ = 0.035
1
10
100
(a)
Im R1
λ =10
(b)
Re R5
λ=0.07
(c)
Im R5
λ = 1
(d)

Fig. 12

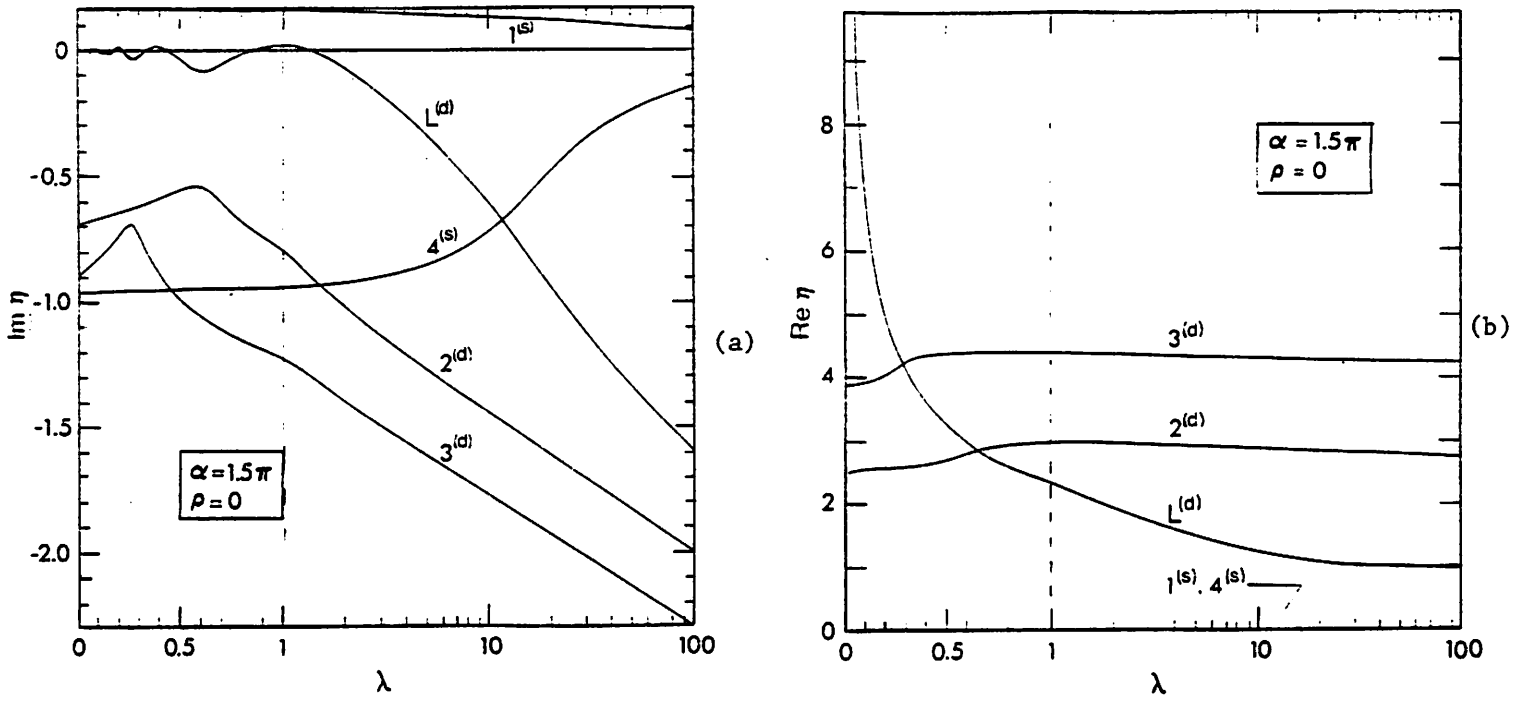
Im η
λ
α=1.5π
ρ=0
1(s)
L(d)
4(s)
2(d)
3(d)
(a)
Re η
α = 1.5π
ρ = 0
3(d)
2(d)
L(d)
1(s), 4(s)
(b)

Fig. 13

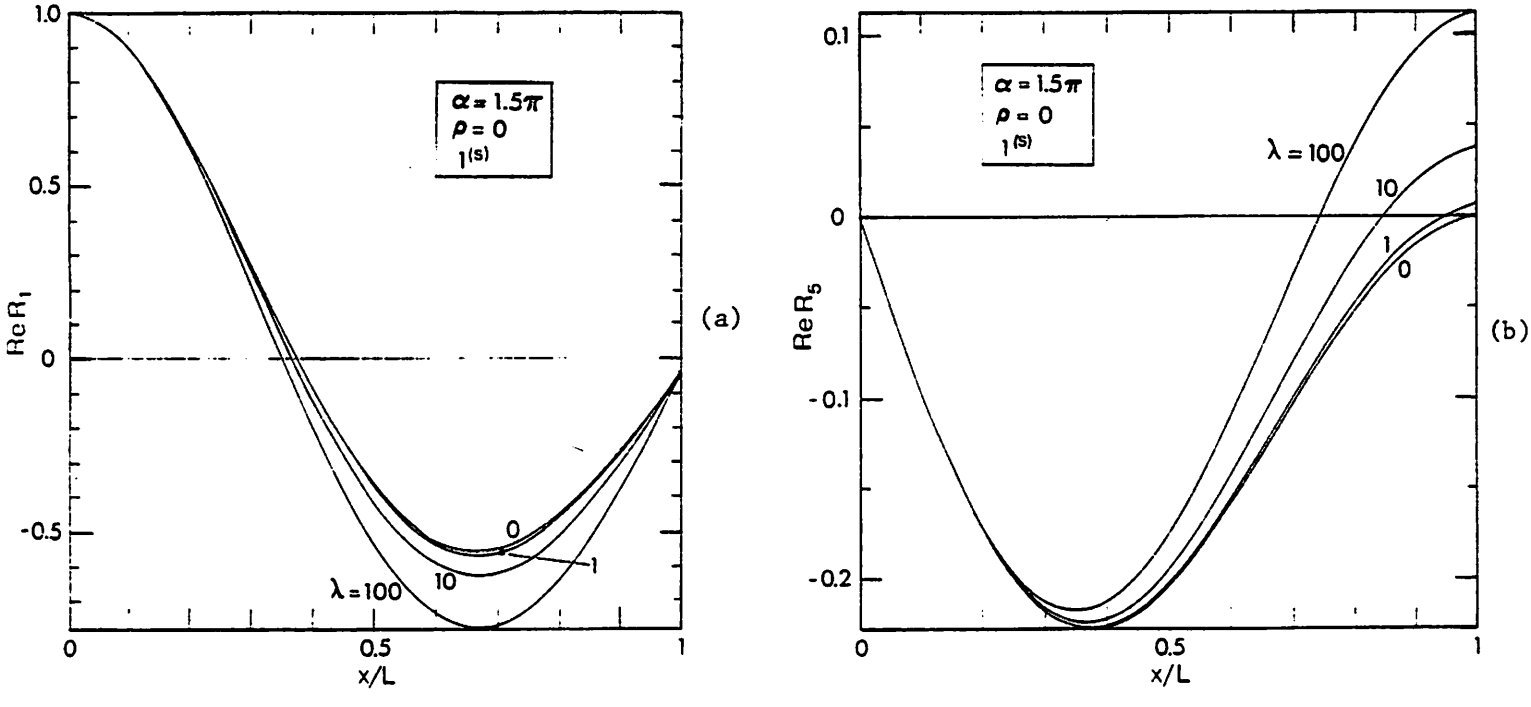
Re R1
x/L
α = 1.5π
ρ = 0
1(s)
λ = 100
10
1
0
(a)
Re R5
(b)

Fig. 14

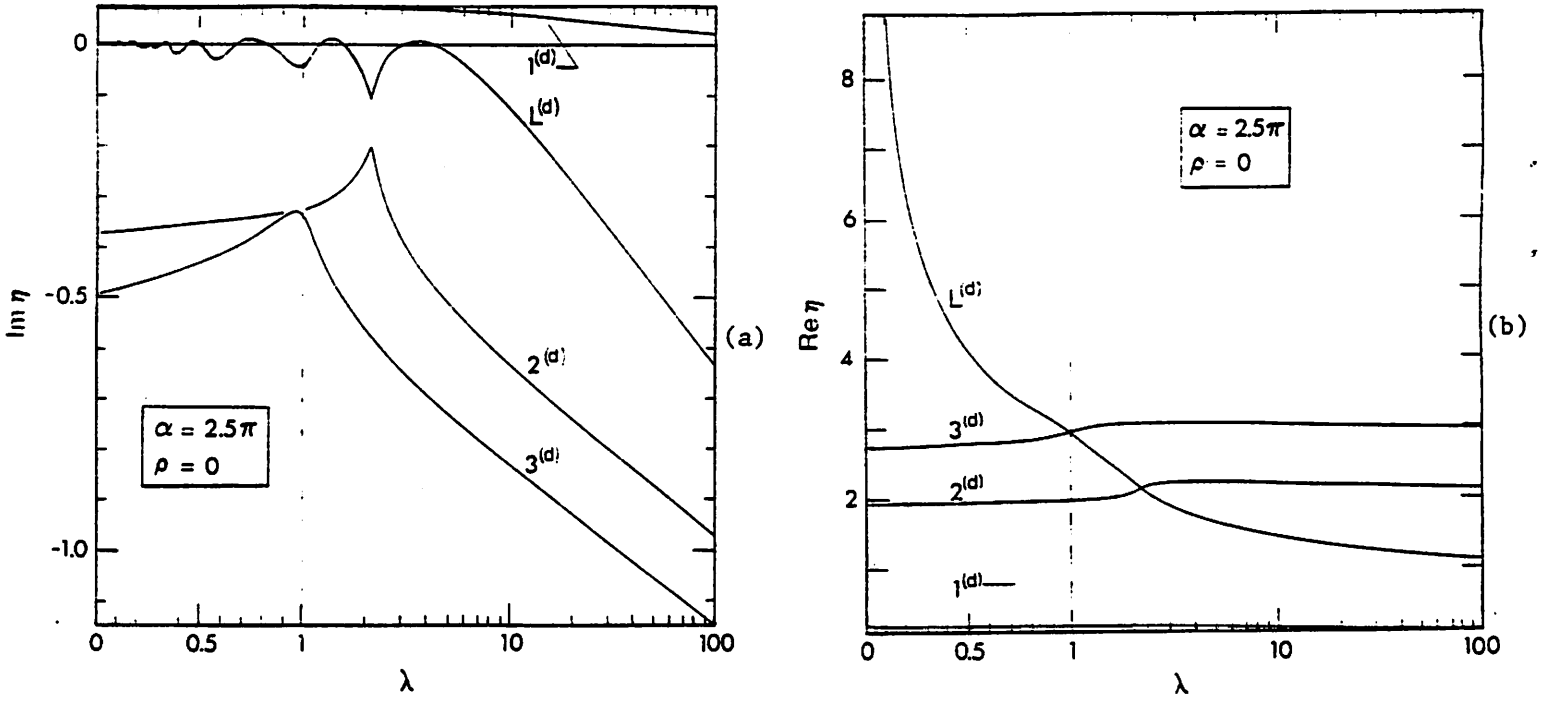
0
-0.5
-1.0
Im η
1(d)
L(d)
2(d)
3(d)
α = 2.5π
ρ = 0
0
0.5
1
10
100
λ
(a)
8
6
4
2
Re η
L(d)
3(d)
2(d)
1(d)
α = 2.5π
ρ = 0
0
0.5
1
10
100
λ
(b)

Fig. 15

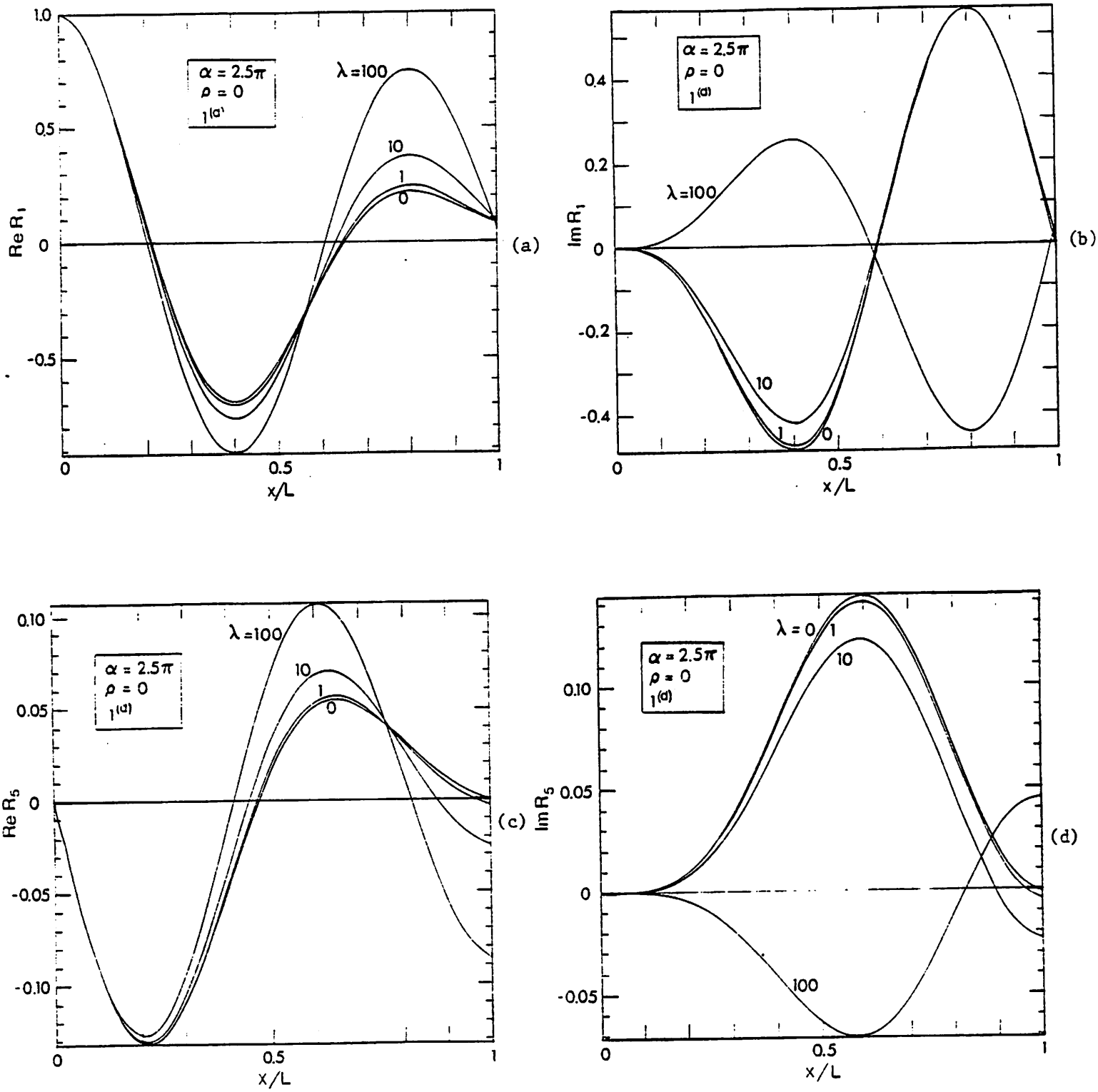

Fig. 16